

# Seismic Source Processes of 25 Earthquakes ( $M_w > 5$ ) in the Gulf of California

Eduardo Huesca-Pérez<sup>\*1</sup> , Edahí Gutierrez-Reyes<sup>1</sup> , and Luis Quintanar<sup>2</sup> 

## ABSTRACT

The Gulf of California (GoC) is a complex tectonic boundary that has been instrumented in the past several decades to record broadband seismograms. This volume of data has allowed us to study several source parameters systematically. Before, only a few source parameters of earthquakes greater than magnitude five had been studied in the GoC area. We re-examined the focal mechanisms of several earthquakes in the southern GoC that occurred over the last 20 yr using local-regional distance broadband seismograms. These focal mechanisms were then used as input data to retrieve the time-space history of the rupture for each earthquake. This work contributes to the study of 25 rupture-process models computed with the method proposed by Yagi *et al.* (1999). To investigate more about the nature of the seismicity in the GoC, we also calculated the non-double-couple component of moment tensors for 45 earthquakes. Previous studies (e.g., Ortega *et al.*, 2013, 2016) have shown that non-double-couple components from moment tensors in this region are associated with complex faulting, suggesting that oblique faults or several parallel faults are interacting simultaneously. Our results show that, at least for moderate earthquakes ( $5 < M < 6$ ), rupture processes in the GoC show a complex interaction between fault systems. It is revealed on the important contribution of non-double-couple component obtained in the full moment tensor analysis.

## KEY POINTS

- Rupture process of 25 earthquakes in the Gulf of California.
- Full moment tensors in the Gulf of California Extensional Province.
- Isotropic moment tensors associated with complex faulting in the Gulf Extensional Province.

## INTRODUCTION

The Gulf of California (GoC) is an active rift margin where the North America and the Pacific plates move along each other with a relative motion of about  $\sim 48$  mm/yr (DeMets and Dixon, 1999; Dixon *et al.*, 2000). The GoC can be described as a series of transform faults and spreading centers where a new oceanic crust is created. The tectonic boundary and its faults systems are connected to the south to the East Pacific Rise. As well, the GoC has undergone a series of reorganizations since the Rivera triple Junction migrated some 12 Ma. This reorganization transformed the boundary from oblique to transtensional shearing (Atwater, 1970; Stock and Hodges, 1989).

As well, in the Miocene time, when the East Pacific Rise reached the Baja California trench caused the subduction of the Farallon plate to stop, and it broke into two pieces: The North and South Farallon plates. This stop in the subduction

created a slab window off the Baja California Peninsula (Dickinson and Snyder, 1979; Severinghaus and Atwater, 1990; Thorkelson, 1996). The gap created volcanism related to the postsubduction that can be observed nowadays all along the peninsula (Di Luccio *et al.*, 2014; Huesca-Pérez *et al.*, 2021). The limit between the North America and the Pacific plates moved  $\sim 250$  km inland between 6 and 8 Ma ago with respect to the position of the former subduction back-arc of the Farallon plate. As the limit of the plate was moving, Baja California was separated from the mainland continent, creating the peninsula and the GoC. The peninsula was slowly transferred to the Pacific plate during a period of one million years (Atwater, 1989; Oskin *et al.*, 2001). The Magdalena and Guadalupe microplates were captured by the Pacific plate between 25 and 12 Ma (Coyán *et al.*, 2013), these microplates are remnants of the Farallon plate. It is thought that the transferring process of the peninsula to the

1. CONACYT-Centro de Investigación Científica y de Educación Superior de Ensenada, Unidad La Paz, La Paz, Baja California Sur, Mexico,  <https://orcid.org/0000-0002-6928-6866> (EH-P);  <https://orcid.org/0000-0001-9065-4144> (EG-R); Instituto de Geofísica, Universidad Nacional Autónoma de México (UNAM), Circuito de la Investigación Científica s/n Ciudad Universitaria, Alcaldía Coyoacán, Ciudad de México, Mexico,  <https://orcid.org/0000-0002-0295-5754> (LQ)

\*Corresponding author: ehuesca@gmail.com

Cite this article as Huesca-Pérez, E., E. Gutierrez-Reyes, and L. Quintanar (2022). Seismic Source Processes of 25 Earthquakes ( $M_w > 5$ ) in the Gulf of California, *Bull. Seismol. Soc. Am.* **XX**, 1–20, doi: [10.1785/0120210218](https://doi.org/10.1785/0120210218)

© Seismological Society of America

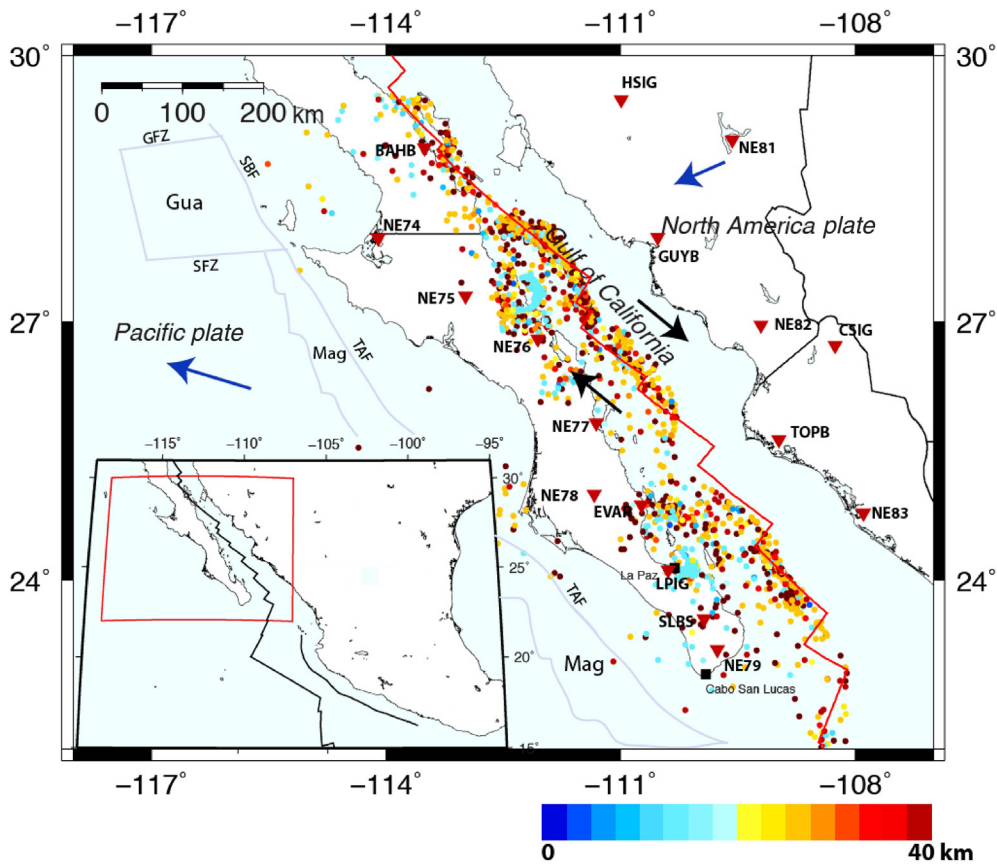


**Figure 1.** Modern tectonic configuration of the Gulf of California extensional province. The red line indicates the boundary between North America and the Pacific plates; this is the boundary where the relative motion is taking place. Two stalled microplates are shown and countered by gray lines: The Guadalupe (Gua) and Magdalena (Mag) microplates that now are part of the Pacific plate. Regional seismicity is reported by Servicio Sismológico Nacional (SSN, National Seismological Service) for the period 1901–2021. The color scale represents the hypocenters depths. The inactive plate boundaries (gray lines) are Tosco—Abreojos fault (TAF), Gua fracture zone (GFZ), and Shirley fracture zone (SFZ). The blue arrows represent the absolute plate motions of the Pacific and North America, whereas the black arrows show the relative plate motions as described by the model NUVEL1A (DeMets and Dixon, 1999). The red inverted triangles represent the seismic stations employed. Inset map shows the region of study (red rectangle). The color version of this figure is available only in the electronic edition.

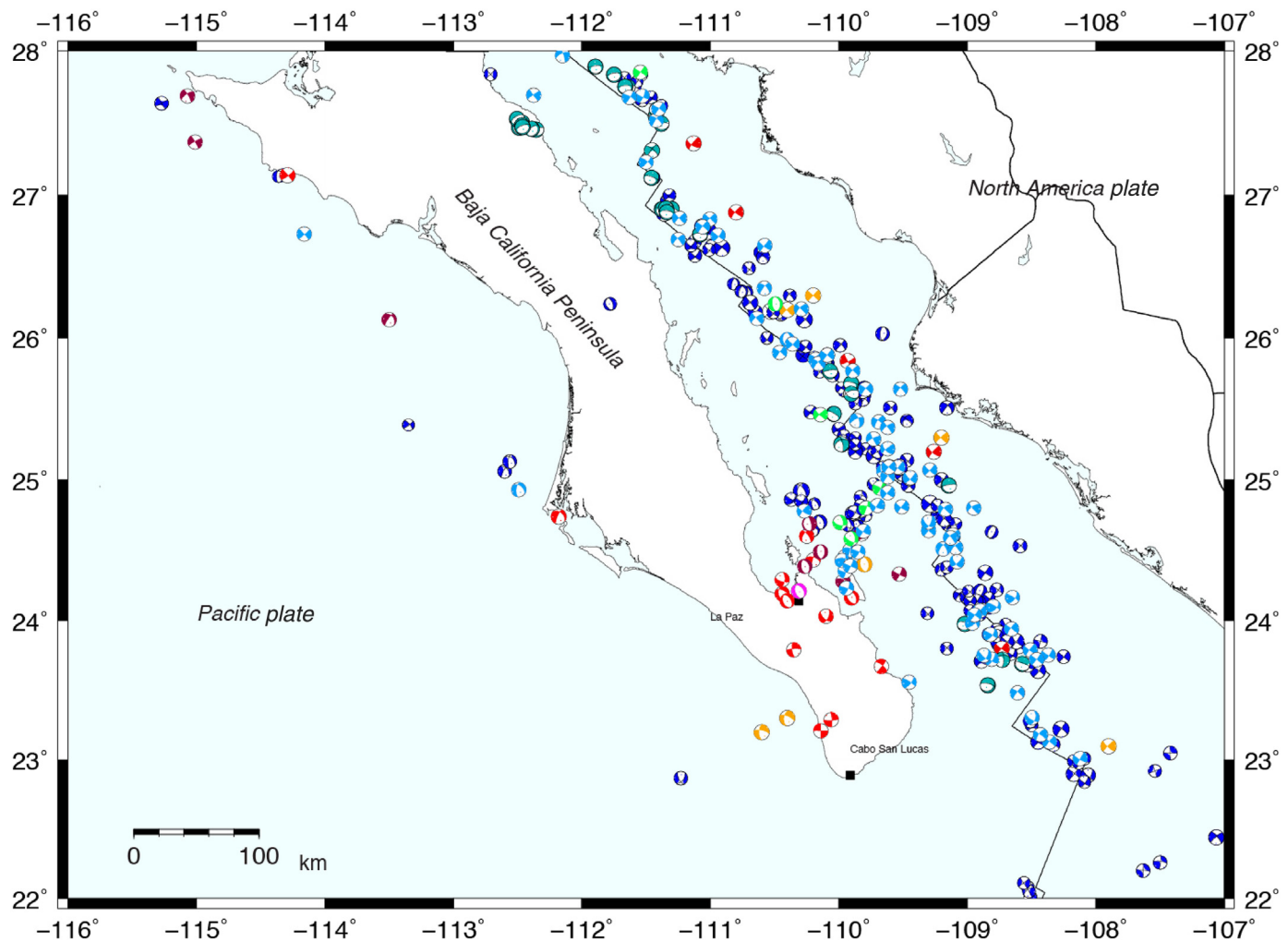
Pacific plate maybe not be finished yet due to velocity differences present (Dixon *et al.*, 2000). To the west of the peninsula, the ancient Farallon paleotrench (the Tosco—Abreojos fault) is accommodating strike-slip deformation that is thought to be related to the differences of motion between the Pacific and the North America plate (Dixon *et al.*, 2000; Marsaglia, 2004; Michaud *et al.*, 2006). Modeling of the motion of the Pacific plate has revealed that since 12.3 Ma it has moved around 720 km to the northwest with respect to the North America plate (Atwater and Stock, 1998). It is thought that this motion has split the deformation into two belts on both sides of the Baja California peninsula that resulted in the opening of the GoC by orthogonal rifting and dextral shear. Around 350 km of displacement has been accommodated over 6 Ma along faults west of the peninsula before it was finally established the transtensional regime observed today. The modern configuration of

plate boundaries of the GoC area is shown in Figure 1. The figure describes the relative motion between plates, the microplates of Guadalupe and Magdalena, and the seismicity reported by Servicio Sismológico Nacional (Servicio Sismológico Nacional [SSN], 2021) catalog in the Gulf area since 1901 (colored dots).

Focal mechanisms have been reported for the Gulf Extensional Province since the decade of the 1960s. This historical information is compiled in Figure 2 and comes from several authors (e.g., Global Centroid Moment Tensor [Global CMT] Dziewonski *et al.*, 1981; Goff *et al.*, 1987; Fletcher and Munguía, 2000; González *et al.*, 2006; Munguía *et al.*, 2006, 2016; Ekström *et al.*, 2012). The focal mechanisms show, in general, a strike-slip dextral movement in central GoC, normal faulting in extensional basins and near the Gulf's peninsula coast. In addition, normal faulting is observed in the seismicity detected in the Magdalena and Guadalupe microplates. To complement the historical information, new focal mechanisms were included using local

data based on the International Seismological Center (ISC) catalog since the year 2000. The historical information is shown in Figure 2 (light blue focal mechanisms).

Source parameters have been studied in the GoC by several authors for medium-sized earthquakes (magnitudes from 5.2 to 6.2). Medium-sized earthquakes are typical in the Gulf of California (Rebollar *et al.*, 2001; Trampert *et al.*, 2003; Clayton *et al.*, 2004). Castro *et al.* (2021) compiled a catalog from 1901 to 2018 for the Gulf Extensional Province and found minimum magnitude completeness of **M** 3.6 and a maximum of **M** 7.2. For medium-sized earthquakes, we can give the following examples that have been studied such as the Delfín earthquake of 26 November 1997 of magnitude 5.5 (Rebollar *et al.*, 2001) and the Loreto earthquake of 12 March 2003 (López-Pineda and Rebollar, 2005). In addition, Rodríguez-Lozoya *et al.* (2008) studied four medium-sized earthquakes using regional and



teleseismic broadband data: The 12 March 2003  $M$  5.7 Loreto, 12 November 2003  $M$  5.3 Angel de la Guardia, 24 September 2004  $M$  5.2 San Lorenzo, and 22 February 2005  $M$  5.6 Topolobampo earthquakes. As stated before, large-magnitude earthquakes of  $\sim 7.0$  have also occurred in the GoC like the one of 7.0 that shacked the Guaymas and Farallon basin (Pacheco and Sykes, 1992; López-Pineda and Rebollar, 2005).

Few source parameters of moderate earthquakes' magnitude ( $M > 5$ ) have been studied in the GoC area (e.g., Rodríguez-Lozoya *et al.*, 2008; Quintanar *et al.*, 2019). In this work, we contribute with 25 rupture-process models. These earthquakes were taken from the ISC catalog for the southern part of the GoC, and we kept the ones whose focal mechanisms could be recomputed using local data and allowed to perform a source rupture inversion with a local velocity model (Table 1). Those focal mechanisms were the input to the inversion program (Table 2; Fig. 3). In addition, using the Papazachos *et al.* (2004) relationships, we estimate the actual rupture area and the stress drop. To finish, we also investigate the non-double-couple component of moment tensors in the GoC. Several studies have proved (e.g., Ortega *et al.*, 2013, 2016) that moment tensors in the GoC have important non-double-couple components, suggesting that oblique faults and/or several

**Figure 2.** Historical focal mechanisms reported in the literature since 1963. The colored quadrants of the focal mechanisms are the compressive and white the extensive. The different colors represent different sources of information. Dark blue indicates Global Centroid Moment Tensor (Global CMT), light red indicates Munguía *et al.* (2006, 2016), dark green indicates Sumy *et al.* (2013), orange indicates Molnar (1973), dark red indicates Goff *et al.* (1987), purple indicates Fletcher and Munguía (2000), bright green indicates Castro *et al.* (2017), and light blue indicates International Seismological Center (ISC) catalog for the period 2000–2020 (this study, computed with local data). The color version of this figure is available only in the electronic edition.

TABLE 1  
**Velocity Model Used to Compute Green's Functions (Ortega *et al.*, 2013)**

| Thickness (km) | $V_p$ (km/s) | $V_s$ (km/s) | Density (g/cm <sup>3</sup> ) |
|----------------|--------------|--------------|------------------------------|
| 2.0            | 4.0          | 2.3          | 2.3                          |
| 5.0            | 6.0          | 3.4          | 2.4                          |
| 8.0            | 6.4          | 3.6          | 2.7                          |
| 55.0           | 7.5          | 4.2          | 3.1                          |
| 22.0           | 7.5          | 4.2          | 3.2                          |
| 23.0           | 7.6          | 4.3          | 3.2                          |

TABLE 2

**Earthquake Parameters and Focal Mechanisms Obtained in This Study Used as Input to Compute Source-Rupture Inversion**

| <b>Origin Time</b><br><b>(yyyy/mm/dd hh:mm:ss)</b> | <b>Latitude</b><br><b>(°)</b> | <b>Longitude</b><br><b>(°)</b> | <b>Depth</b><br><b>(km)</b> | <b>Magnitude</b><br><b>(<math>M_w</math>)</b> | <b>Strike</b><br><b>(°)</b> | <b>Dip</b><br><b>(°)</b> | <b>Rake</b><br><b>(°)</b> | <b>Number</b><br><b>of Event</b> |
|--|-------------------------------|--------------------------------|-----------------------------|---|-----------------------------|--------------------------|---------------------------|----------------------------------|
| 2003/07/02 05:11:34                                | 22.90                         | -108.19                        | 10                          | 5.6   | 31, 121                     | 89, 76                   | -14, -179                 | 1                                |
| 2004/02/09 09:03:46                                | 24.93                         | -112.49                        | 10                          | 5.3   | 185, 310                    | 61, 44                   | -55, -136                 | 2                                |
| 2004/02/18 10:59:19                                | 23.64                         | -108.82                        | 10                          | 5.8   | 30, 126                     | 73, 72                   | -19, -163                 | 3                                |
| 2005/02/22 19:15:49                                | 25.77                         | -109.89                        | 10                          | 5.4   | 312, 221                    | 86, 82                   | -172, -4                  | 4                                |
| 2005/06/05 08:28:50                                | 23.67                         | -108.37                        | 10                          | 5.6   | 124, 34                     | 88, 79                   | -169, -3                  | 5                                |
| 2006/01/04 01:05:08                                | 27.97                         | -112.15                        | 10                          | 5.2   | 341, 245                    | 77, 66                   | -155, -15                 | 6                                |
| 2006/07/30 01:20:59                                | 26.86                         | -112.21                        | 10                          | 5.8   | 319, 228                    | 85, 75                   | -165, -5                  | 7                                |
| 2007/03/13 02:59:01                                | 26.14                         | -110.64                        | 10                          | 5.9   | 140, 230                    | 88, 75                   | 165, 2                    | 8                                |
| 2007/09/01 19:14:23                                | 24.99                         | -109.66                        | 10                          | 6.0   | 117, 26                     | 86, 81                   | -171, -4                  | 9                                |
| 2009/07/03 10:00:16                                | 25.22                         | -109.62                        | 17                          | 5.9   | 231, 187                    | 82, 63                   | 27, 171                   | 10                               |
| 2010/10/20 06:58:14                                | 24.52                         | -109.09                        | 10                          | 5.8   | 317, 224                    | 82, 69                   | -159, -8                  | 11                               |
| 2010/10/20 04:09:43                                | 24.59                         | -109.13                        | 10                          | 5.9   | 320, 226                    | 82, 69                   | -159, -8                  | 12                               |
| 2010/10/21 17:53:13                                | 24.79                         | -109.17                        | 14                          | 6.6   | 134, 44                     | 90, 77                   | 155, 180                  | 13                               |
| 2011/07/26 17:44:21                                | 25.09                         | -109.54                        | 17                          | 6.1   | 40, 309                     | 86, 80                   | -10, 175                  | 14                               |
| 2012/04/12 07:15:49                                | 28.84                         | -113.13                        | 10                          | 7.1   | 131, 40                     | 74, 87                   | -177, -16                 | 15                               |
| 2012/09/25 23:45:24                                | 24.77                         | -110.18                        | 8.1                         | 6.2   | 180, 329                    | 54, 40                   | -71, 114                  | 16                               |
| 2012/10/08 06:26:23                                | 25.09                         | -109.61                        | 17                          | 5.9   | 129, 219                    | 89, 87                   | 177, 1                    | 17                               |
| 2013/10/19 17:54:57                                | 25.96                         | -110.36                        | 15                          | 6.6   | 134, 43                     | 87, 83                   | -173, -3                  | 18                               |
| 2014/08/10 18:46:17                                | 27.68                         | -111.63                        | 10                          | 5.5   | 32, 300                     | 83, 78                   | 12, 172                   | 19                               |
| 2014/10/08 02:40:52                                | 23.79                         | -108.51                        | 7.1                         | 6.1   | 217, 126                    | 84, 81                   | 9, 173                    | 20                               |
| 2015/08/07 04:35:01                                | 24.04                         | -108.94                        | 10                          | 5.4   | 306, 36                     | 86, 85                   | 175, 4                    | 21                               |
| 2015/09/13 07:57:33                                | 24.81                         | -109.51                        | 10                          | 5.6   | 36, 126                     | 90, 90                   | -12, 180                  | 22                               |
| 2015/09/13 08:14:08                                | 24.91                         | -109.62                        | 10                          | 6.7   | 38, 128                     | 89, 89                   | -12, -178                 | 23                               |
| 2017/03/29 15:15:23                                | 25.71                         | -110.02                        | 17                          | 5.6   | 128, 218                    | 90, 88                   | 178, 1                    | 24                               |
| 2018/01/19 16:17:42                                | 26.68                         | -111.11                        | 10                          | 6.3   | 218, 308                    | 86, 84                   | -6, -175                  | 25                               |

In addition, the auxiliary nodal plane is given after comma of each event.

parallel faults are interacting simultaneously. In this study, we present new results of the earthquake source characteristics. These results show that the seismicity in the GoC has a relatively simple time–space history of the rupture, but their focal mechanisms show some complexity observed as non-double-couple components of the moment tensor. This characteristic is observed in small and moderate size earthquakes, indicating that they are equally complex (Ortega *et al.*, 2013). This suggests that deformation in the GoC area is not only being accommodated by the principal transform fault but also by secondary parallel or perpendicular faults that induce the interaction of multiple fault systems during the earthquake process.

## DATA AND METHOD

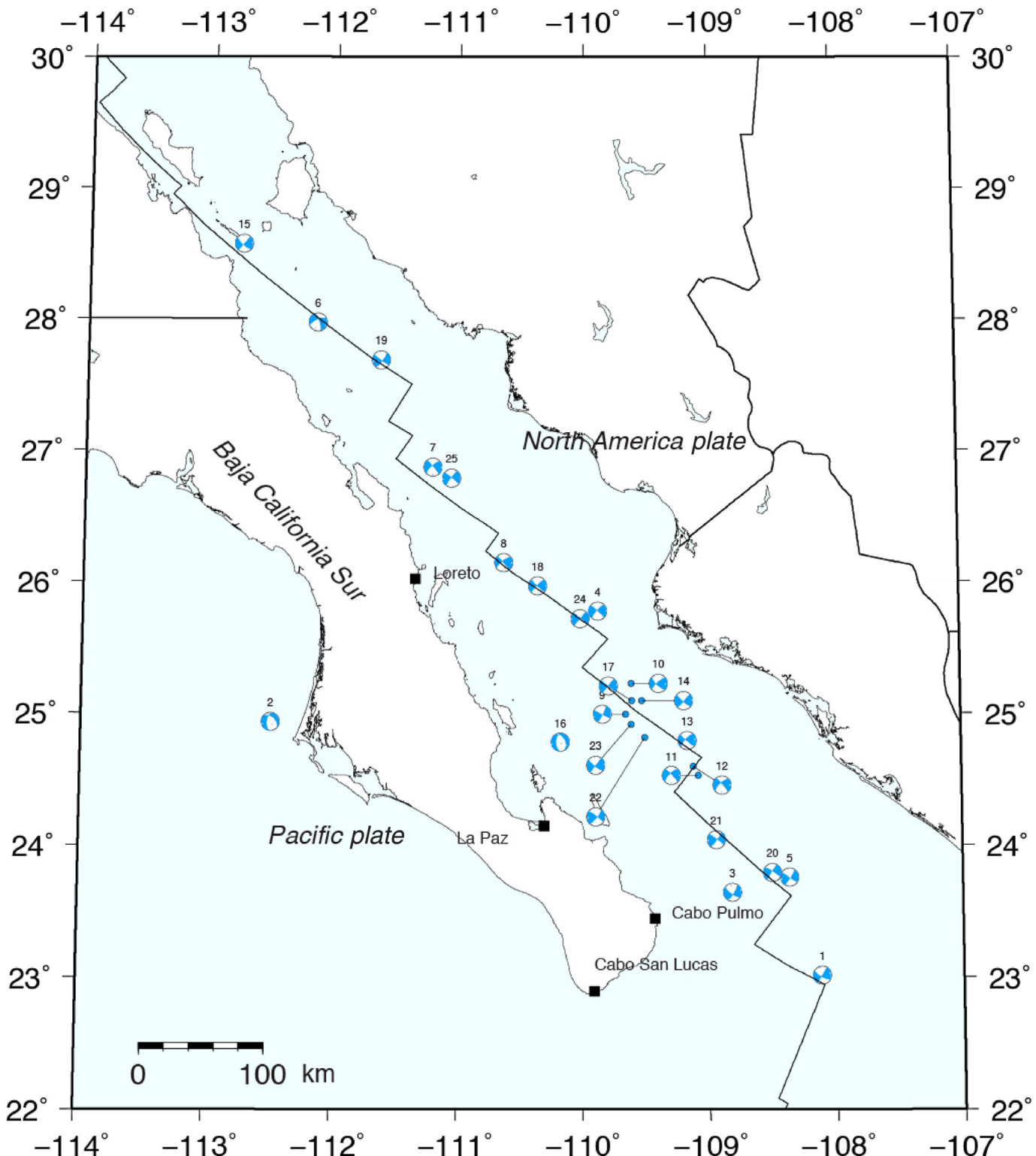
### Data

The regional seismic waveform data were obtained from several sources. The station locations of Network of Autonomously Recording Seismographs (NARS-Baja) and the Red Sismológica de Banda Ancha del Golfo de California (RESBAN) networks International Federation of Digital Seismograph Networks network codes: NARS (NR), Red Sismológica de Banda Ancha (RB), respectively, are shown in Figure 1 (red inverted triangles). Waveform data were instrument corrected and filtered to displacement for regional moment tensor inversion (100–50 s

period) and velocity ground-motion units for rupture model inversion (0.02–0.5 Hz). Hypocenter information was downloaded from ISC earthquake catalogs, and seismograms were downloaded using the Incorporated Research Institutions for Seismology (IRIS)-Wilber 3 system for the period 2000–2018. The 1D velocity model was derived from Ortega *et al.* (2013) and used to compute Green's functions (Table 1).

### Method

**Moment tensor inversion.** Moment tensors for the earthquakes listed in Table 2 were recomputed using local data and a local velocity model. The procedure uses the algorithm proposed by Dreger and Helmberger (1990, 1991, 1993). The full moment tensor solution is computed in the time domain from the inversion of the regional long-period filtered three-component waveform data using Green's functions computed from the 1D velocity model (Table 1). The tensor is then decomposed into three eigenvalues, which are used to estimate the double couple (DC), compensated linear vector dipole (CLVD), and the isotropic component (ISO) (Jost and Herrmann, 1989). In addition, Green's functions are calculated to compute synthetic seismograms using the method of Saikia (1994). This frequency and wavenumber integration method uses the efficient Filon's quadrature algorithm. The fit between



synthetics and observed seismograms is constrained to the deviatoric tensor and neglects the isotropic part. The best solution is determined by the variance reduction (VR), which must be maximum when the depth is varied at 2 km step.

**Source rupture process inversion.** To investigate the rupture process over a fault of earthquakes of the GoC, we used the

**Figure 3.** Map showing the location of the 25 epicenters and their focal mechanisms of Table 2. The numbers above each focal mechanism plot are their position within the catalog. The black continuous line represents the plate boundary between the Pacific and the North America plates. The colors of the focal mechanism plots represent the compressive (blue) and extensive (white) quadrants. The color version of this figure is available only in the electronic edition.

[Yagi et al. \(1999\)](#) method and the formulation of [Yoshida \(1989, 1992\)](#) and [Hartzell and Heaton \(1983\)](#). To compute the spatio-temporal rupture process, a grid is established over the fault plane. The fault surface is segmented into  $M \times N$  subfaults with length  $x$  and width  $y$ . In each subfault, the slip-rate function is computed as a series of overlapping triangles functions with a rise time  $\tau$  of 1.2 s. Slip vectors at each subfault are computed. Near-field ground-motion Green's functions are calculated by the algorithm proposed by [Kohketsu \(1985\)](#), for which the discrete wave-number is used. Stability in the solution can be obtained by applying smoothing constraints on the slip distribution to space, time, and slip angle.

A least-squares method is then applied whose solution will depend on values obtained on relative weights of constraints. These weights are determined by the [Akaike \(1980\)](#) method, which adopts the minimum Bayesian information criterion (ABIC). This is a statistical criterion that uses the theorem of maximum entropy to the Bayesian statistics. For the smoothness regularization, it is sought a model that can minimize the data misfit and the model roughness. It means that ABIC works as an index of the maximum likelihood of the obtained model. The optimum smoothness is given by minimizing ABIC that makes the selection and convergence of the final smoothness in the objective of the procedure. Each of the focal mechanism obtained is reported in Table 2 in the [Results](#) section and were analyzed using [Yagi et al. \(1999\)](#) algorithm.

**Non-double-couple moment tensors in the GoC.** We investigate the non-double-couple part of the moment tensor. The full moment tensor is a mathematical representation of six independent variables. However, this mathematical representation is, in general, simplified by assuming that the isotropic part is zero. This assumption is valid in tectonic regimes where the slip mostly occurs at the fault surface. In contrast, significant non-double-couple components have been found in transform systems, such as the GoC (e.g., [Ortega et al., 2013, 2016](#)). Here, we investigate full moment tensors in the Gulf of California Extensional Province using the methodology proposed by [Ortega et al. \(2013, 2016\)](#). This method analyzes the earthquake source complexity using a formulation that relates the elastics constants with the angle between the slip and the fault normal vector. The method obtains the proportion of volume change and the constant of volume shear component as numerical indicators of the complexity of the source. The normal vector  $\theta$  indicates that an earthquake is more complex, because it deviates from  $\pi/2$  or as the shear component  $T$ , or the volume change  $k$  deviates from zero. The parameters mentioned before are the eigensolutions of the full moment tensor. The full moment tensor is computed using waveform modeling (e.g., [Minson and Dreger, 2008; Ford et al., 2009](#)) in which the inversion is performed in two steps: (1) the synthetic and observed waveforms are aligned so the S-wave arrival-time align; and (2) the moment tensor is computed constraining a correlation factor between the observed and synthetic with a time shift less than 50 s.

Synthetic seismograms were computed at different depths varying the hypocenter from 2 to 20 km, each step of 2 km computing the Green's functions with the model of [Ortega et al. \(2013\)](#). Synthetic and observed signals were filtered between 0.02 and 0.04 Hz. The inversion to obtain the full moment tensors are performed following the methodology of [Ford et al. \(2009\)](#) and [Ortega et al. \(2013\)](#) in which it is proposed as a measure of the fit quality of the VR:

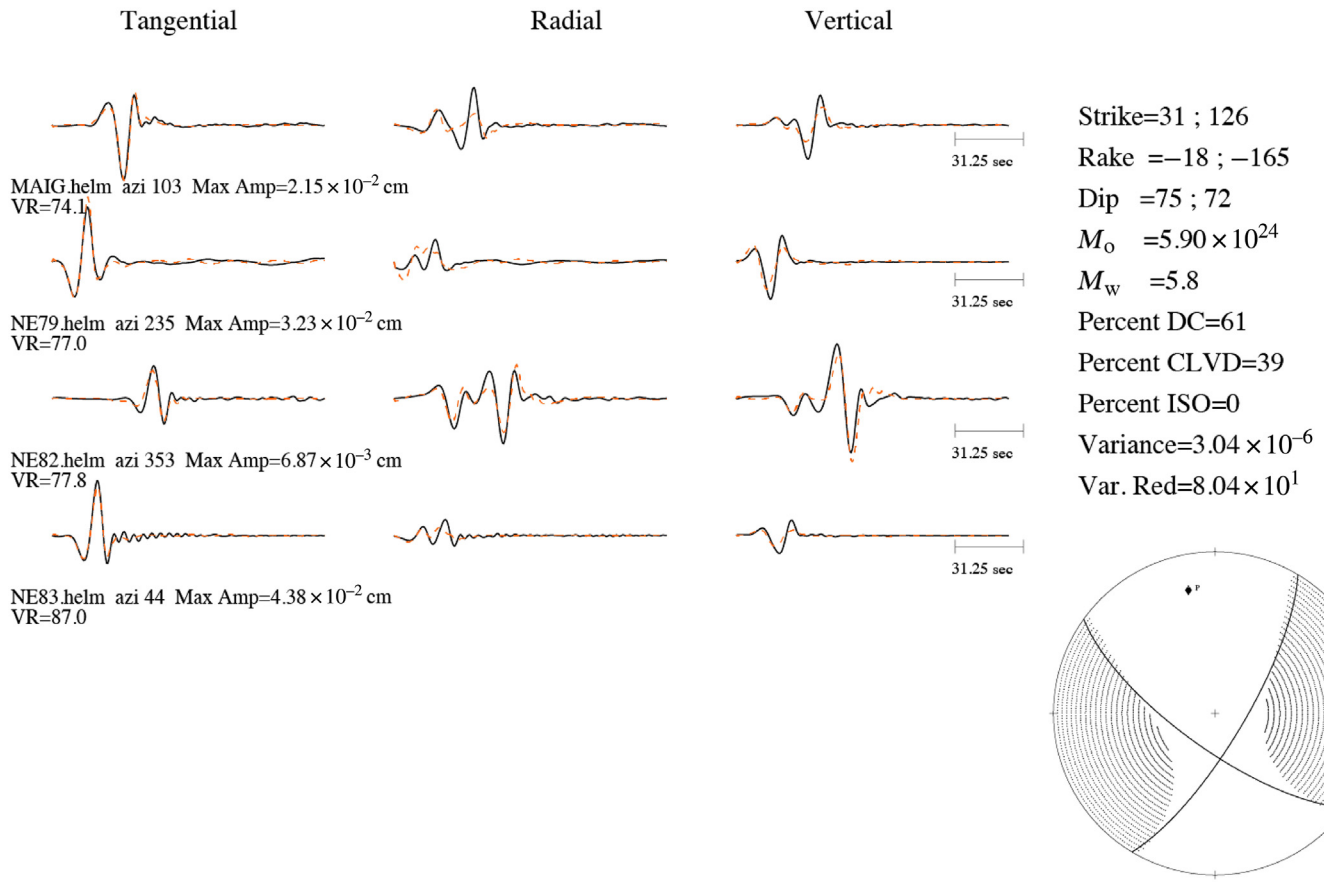
$$VR = \left[ 1 - \sum_i \sqrt{(d_i - s_i)^2} / \sqrt{d_i^2} \right] \times 100, \quad (1)$$

in which  $d$  and  $s$  are the data and synthetics, respectively. For each reinversion of the moment tensor with depth, the VR was obtained to investigate at which step the VR is maximum. The VR will be maximum when the error is minimum. The regularized matrix used is processed using least squares that will minimize the errors between the observed and synthetics. After the moment tensor is computed, the characteristic equation is solved; so it is possible to get the eigenvalues and eigenvectors using an iterative Jacobi method ([Ortega et al., 2013](#)). In general, these types of focal mechanisms are a mechanical representation of DCs and lineal dipoles ([Ortega et al., 2013](#)). The moment tensor of six components represents a general source model in which a pair combination of eigenvalue–eigenvector represents a linear dipole giving a combination of three orthogonally oriented pairs of forces acting in opposite directions. In the deviatoric form, the tensor is parameterized by the scalar seismic moment and three Euler angles for the fault plane. These planes are the strike, dip, and rake. To represent these full moment tensors, the source type plot proposed by [Hudson et al. \(1989\)](#), which is a simple representation of the source is used. The plot is constructed choosing the parameter  $k$ , which is a measure of the size of the dilatational component (the isotropic part), and the constant  $T$  as a second parameter that represents the constant-volume component related to the CLVD. The Hudson plot represents the failure process in terms of shear, tensile, explosion, or implosion ([Hudson et al., 1989](#)).

## RESULTS

### Examples of rupture processes

In this section, we show two examples of the inversions performed. First, we computed the focal mechanism using [Dreger and Helmberger \(1990, 1991, 1993\)](#), as it was described in the [Moment tensor inversion](#) section. From this procedure, we obtained 25 high-quality focal mechanisms that are listed in Table 2 and plotted in Figure 3, and the compressive quadrants are colored in blue. These focal mechanisms will be the input to analyze their rupture process whose methodology was described in the previous section. Table 2 is ordered chronologically with the oldest earthquake being number one and the latest being number 25. The columns indicate, origin time, epicenter latitude and longitude, depth, moment magnitude ( $M_w$ )



and, focal mechanism (strike, dip, and rake). Both nodal plane solutions are registered. The first column of each focal mechanism is the geological solution constrained by the bathymetry of the GoC and used to compute the rupture inversion; the second column is the auxiliary nodal plane.

We performed the moment tensor inversion of earthquake 3 of Table 2 using four stations that recorded this event. The signals were band-pass filtered between 0.01 and 0.05 Hz. The fault-plane solution is shown along with the synthetics and observed fit in Figure 4, whose parameters indicate a predominantly strike-slip event with strike = 30, dip = 73, and rake = -19, and a hypocenter depth of it is 10 km. In addition, it has a DC component of 61% and a CLVD of 39%. To perform the inversion for the slip distribution shown in Figure 5, which is a 5.8 magnitude earthquake, data from local seismic stations were used. The input focal mechanism needed to compute the inversion is shown in Figure 4. Figure 5 shows the source parameters that include the focal input mechanism, the moment rate function, the fault-plane solution, and the observed (black continuous line) and the synthetic (red continuous line) seismograms. For this event, in particular, it was not possible to use teleseismic data, because it was poorly recorded at teleseismic distances. We limited our inversion to regional data due to low signal levels compared to background noise levels at larger distances. The event is located in the GoC in front of Cabo Pulmo, near the peninsula of Baja California

**Figure 4.** Time-domain moment tensor inversion of event 3 of the catalog of Table 2. The observed tangential, radial, and vertical waveforms are shown as solid black lines, whereas the red dashed lines show the synthetic seismograms in displacement. The results of the inversion are presented along with the focal mechanism. The color version of this figure is available only in the electronic edition.

coast. The inversion was performed using a fault-plane area segmented into  $7 \times 4$  subfaults, each with an area of  $4 \times 4$  km, that covers a total area of  $336 \text{ km}^2$ . The slip-rate function on each subfault was computed using four overlapping triangles with a rise time of 1.2 s. We tested several rupture velocities in a range from 2.8 to 3.5 km/s. A rupture velocity of 3.0 km/s showed a minimum variance between observed and synthetic seismograms. To perform the inversion, we used 50 s of the signal leaving 10 s before the arrival of the P wave, and the signals were band-pass filtered using a Butterworth filter between 0.03 and 0.5 Hz.

The source rupture process shows several patches of seismic moment release indicating that the rupture is complex with many asperities. In addition, Figure 5 shows that the duration of the moment rate function was 7 s. According to the position of the patches, it shows a propagation, first to the northwest, later it continues toward the southeast, and it is reflected in the source time function as a series of peaks. The maximum

### Gulf of California 3

Moment =  $0.2728 \times 10^{18}$ (N·m),  $M_w$  5.6  
 (Strike, Dip, Slip) = (126.0, 72.0, -163.0)

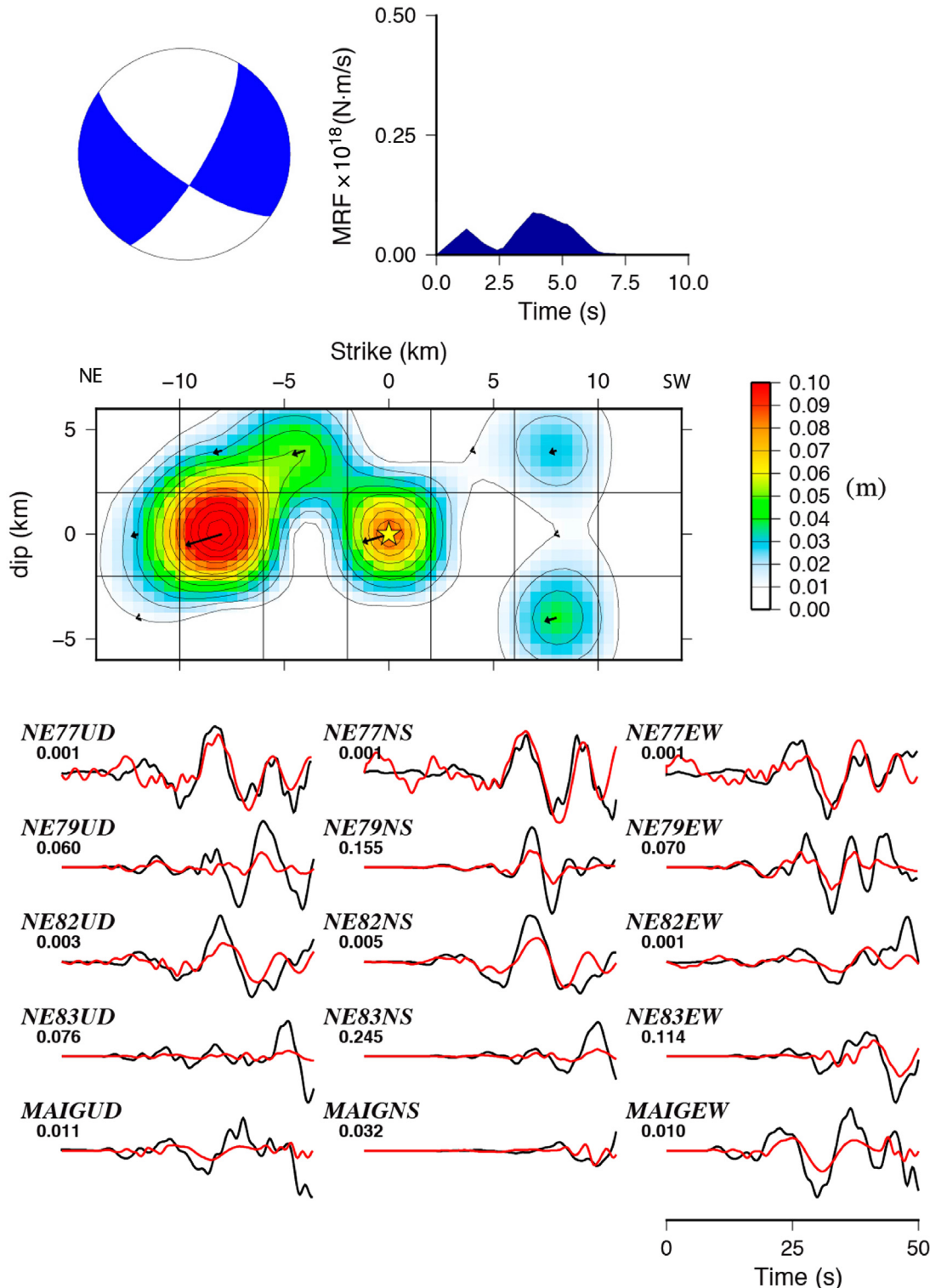


**Figure 5.** The results of the inversion process of event number 3 of Table 2, located in front of Cabo Pulmo in the Gulf of California. The signals were band-pass filtered using a Butterworth filter between 0.03 and 0.5 Hz and a fault plane with subfaults of  $4 \times 4$  km. Focal mechanism, moment rate function, slip displacement, and synthetic (red) and observed waveforms are

shown. The maximum amplitudes (small numbers) are in units of centimeters, and regional waveforms are in microns. The star shows the location of the hypocenter, and black arrows show the direction of the rake. The color version of this figure is available only in the electronic edition.

TABLE 3

**Scalar Moment ( $M_0$ ) Obtained in the Inversion along with Papazachos et al. (2004)**

| Event | $M_0$ (N·m)             | $L$ (km) | $w$ (km) | $S$ (km $^2$ ) | $\Delta\sigma$ (MPa) |
|-------|-------------------------|----------|----------|----------------|----------------------|
| 1     | $1.8550 \times 10^{17}$ | 7.69     | 5.65     | 33.88          | 0.48                 |
| 2     | $1.0600 \times 10^{17}$ | 6.71     | 5.36     | 28.18          | 0.35                 |
| 3     | $2.7280 \times 10^{17}$ | 10.09    | 6.28     | 48.98          | 0.44                 |
| 4     | $1.1370 \times 10^{17}$ | 6.71     | 5.36     | 28.18          | 0.38                 |
| 5     | $2.7530 \times 10^{17}$ | 10.09    | 6.28     | 48.98          | 0.44                 |
| 6     | $9.6820 \times 10^{16}$ | 6.71     | 5.36     | 28.18          | 0.32                 |
| 7     | $5.0040 \times 10^{17}$ | 11.56    | 6.62     | 58.88          | 0.63                 |
| 8     | $5.9320 \times 10^{17}$ | 13.24    | 6.98     | 70.79          | 0.58                 |
| 9     | $1.4750 \times 10^{18}$ | 17.38    | 7.76     | 102.33         | 0.90                 |
| 10    | $4.0840 \times 10^{17}$ | 11.56    | 6.62     | 58.88          | 0.51                 |
| 11    | $3.3750 \times 10^{17}$ | 10.09    | 6.28     | 48.98          | 0.54                 |
| 12    | $4.0740 \times 10^{17}$ | 11.56    | 6.62     | 58.88          | 0.51                 |
| 13    | $7.0940 \times 10^{18}$ | 34.28    | 10.12    | 257.04         | 1.29                 |
| 14    | $1.4910 \times 10^{18}$ | 17.38    | 7.76     | 102.33         | 0.91                 |
| 15    | $6.5030 \times 10^{19}$ | 77.45    | 13.90    | 776.25         | 2.77                 |
| 16    | $2.0820 \times 10^{18}$ | 19.91    | 8.18     | 123.03         | 0.99                 |
| 17    | $7.2990 \times 10^{17}$ | 13.24    | 6.98     | 70.79          | 0.72                 |
| 18    | $8.7680 \times 10^{18}$ | 39.26    | 10.67    | 309.03         | 1.25                 |
| 19    | $2.4200 \times 10^{17}$ | 7.69     | 5.65     | 33.88          | 0.63                 |
| 20    | $1.9920 \times 10^{18}$ | 19.91    | 8.18     | 123.03         | 0.95                 |
| 21    | $1.1640 \times 10^{17}$ | 6.71     | 5.36     | 28.18          | 0.38                 |
| 22    | $2.3980 \times 10^{17}$ | 8.81     | 5.96     | 40.74          | 0.49                 |
| 23    | $9.3750 \times 10^{18}$ | 39.26    | 10.67    | 309.03         | 1.34                 |
| 24    | $1.5800 \times 10^{17}$ | 7.69     | 5.65     | 33.88          | 0.41                 |
| 25    | $3.1000 \times 10^{18}$ | 26.12    | 9.10     | 177.83         | 0.91                 |

$L$ , rupture length (km); RA, rupture area (km $^2$ );  $w$ , down-dip rupture width (km); and  $\Delta\sigma$ , stress drop (MPa).

displacements of the patches are 0.07 m near the hypocenter and 0.10 m to the northwest on the fault plane. A total moment of  $0.2728 \times 10^{18}$  N·m ( $M_w$  5.6) is found. Although a larger area in the inversion was considered in the inversion process the slip distribution encompasses a smaller area. This area was estimated using the empirical relationships of Papazachos et al. (2004) that relate the magnitude of the earthquake with the area fractured, the length, and the width of the fracture. In doing so, we find an area of  $\sim 48.98$  km $^2$  (Table 3).

Assuming a squared fault and using the equation of Haskell (1964),

$$\Delta\sigma = \frac{2M_0}{\pi W^2 L}, \quad (2)$$

and, estimating the rupture length ( $L$ ) and width ( $W$ ) by Papazachos et al. (2004) relationships, it is possible to estimate a stress drop of 0.44 MPa (see Table 3).

Figure 6 shows the results of the moment tensor inversion of earthquake 14 of Table 2 using the algorithm of Dreger and Helmberger (1990, 1991, 1993). For this inversion, we used six local stations that recorded this event. The seismograms were band-pass filtered between 0.01 and 0.05 Hz. In the figure, it is shown the fault-plane solution that is predominantly strike slip with parameters of strike = 40, dip = 86, and rake = -10, with a focal depth of 17 km. In addition, the solution shows that the

moment tensor is predominantly DC (80%) with a CLVD of 20%. In Figure 7, we show the source parameter inversion process of event 14 of Table 2 using local and teleseismic data. The teleseismic stations were chosen to cover the epicenter homogeneously. This event is a magnitude 6.1 and is located well within the GoC showing a strike-slip focal mechanism consistent with the tectonics of the region. The inversion was performed using a fault-plane area segmented into  $5 \times 3$  subfaults, each with an area of  $6 \times 6$  km covering a total area of 540 km $^2$ . The slip-rate function on each subfault was computed using two overlapping triangles with a rise time of 1.2 s, and the slip angle (rake) remained unchanged during the inversion. In addition, we considered several rupture velocities finding that the best for the inversion was a rupture velocity of 3.0 km/s. To perform the inversion, we used 50 s of signal leaving 10 s before the arrival of the  $P$  wave, and the signals were band-pass filtered using a Butterworth filter between 0.03 and 0.3 Hz.

The fault-plane solution shows one elongated patch that is surrounding the hypocenter. This patch is split into two peaks that can be observed in the moment rate function: (1) at the beginning of the rupture with a maximum slip of 0.20 m, and (2) 4 s later, the rupture propagates toward the northwest with a maximum slip of 0.10 m. A third small patch can be observed to the southeast with 0.04 m of displacement occurring 6 s

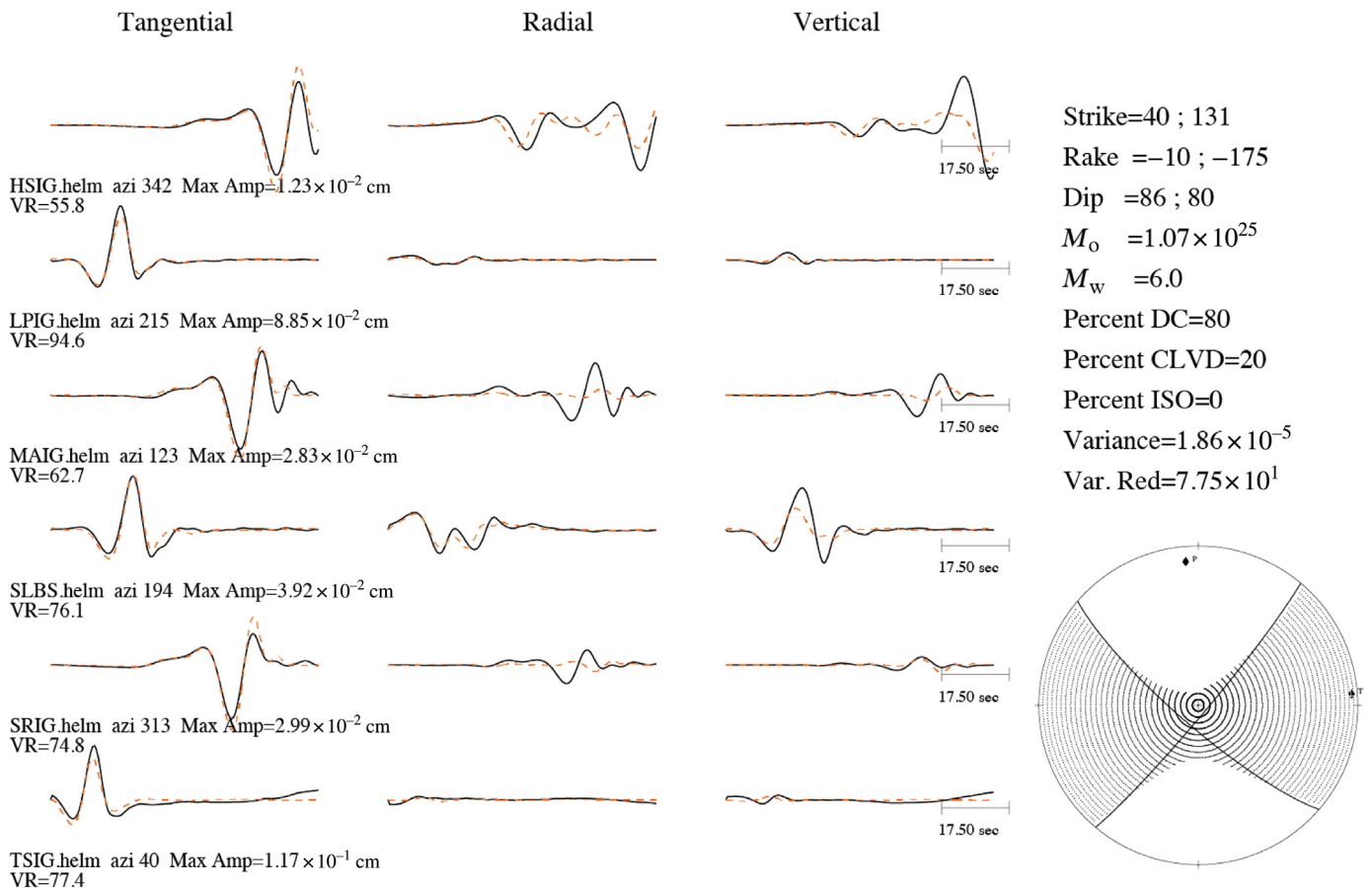


**Figure 6.** Time-domain moment tensor inversion of event 14 of the catalog of Table 2. The red dashed lines show the synthetic seismograms in displacement, whereas the black continuous line shows the observed seismogram. The color version of this figure is available only in the electronic edition.

later. The rupture time of this event can be estimated in 7 s. A total moment of  $0.1170 \times 10^{19}$  N · m ( $M_w$  6.0) is found. To estimate the actual ruptured area, the Papazachos *et al.* (2004) relationships are used, and we found 102.33 km<sup>2</sup> and a stress drop of 0.91 MPa (Table 3).

### Non-double-couple moment tensors in the GoC

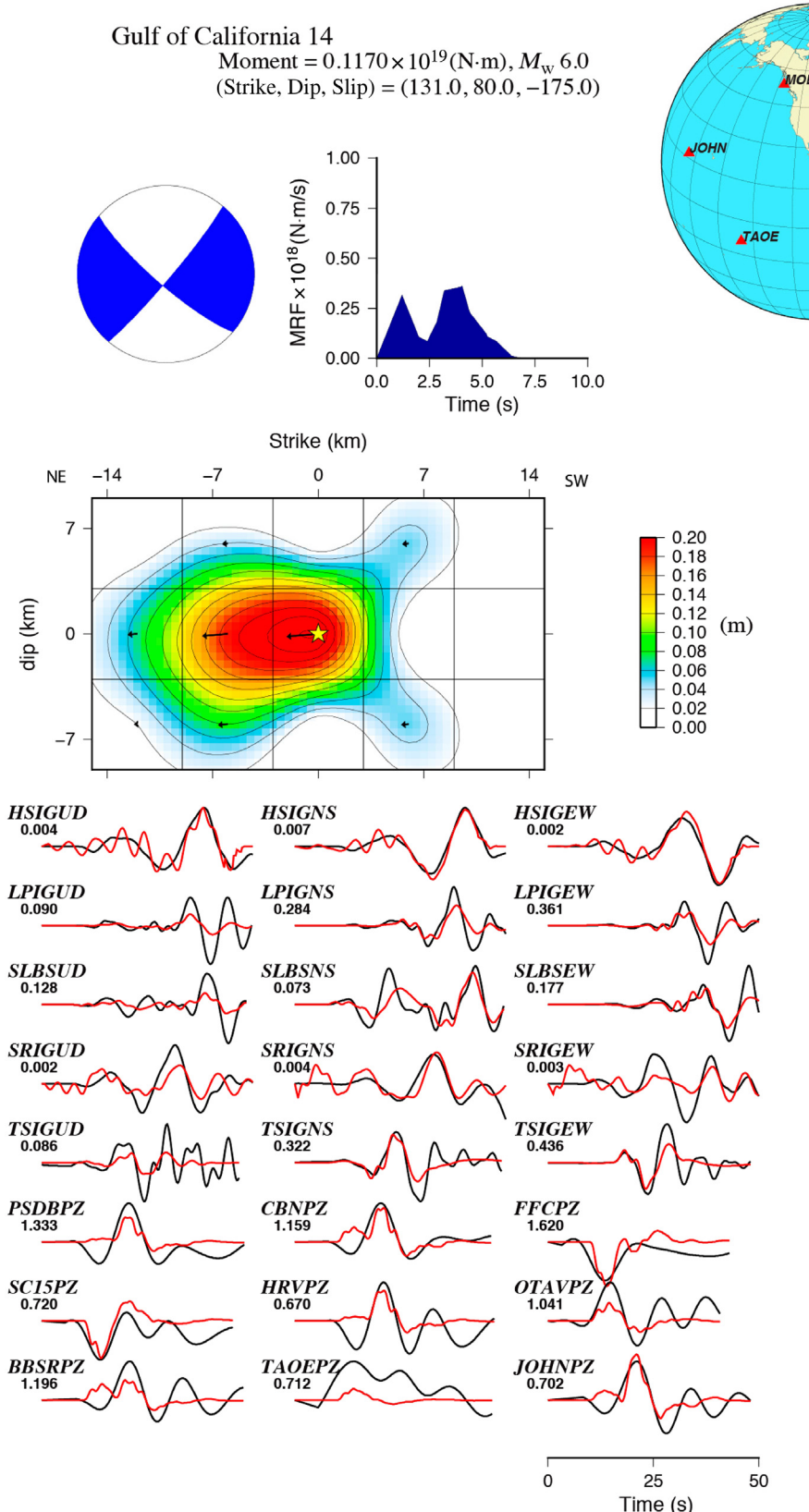
We also investigate the non-double-couple part of the moment tensor of earthquakes in the GoC. The catalog of Table 2 was extended with more events, and it reached 45 earthquakes. The catalog is shown in Table 4. In Figures 8 and 9, we show the inversion of the full moment tensor of events 3 and 14 of Table 2, these events were first inverted fixing the isotropic component to zero. Both plots include the observed (black continuous line) and synthetics (dashed red line) waveforms, the associated DC focal mechanism, and the Hudson plot. Figure 8 shows a variance reduction of 83%, indicating that the fit between observed and synthetics are good with an ISO of 34%. The associated DC fault planes (Fig. 3) almost do not change when they are compared with the nonisotropic inversion. The Hudson plot shows interesting information indicating that event 3 fractured more like a crack.

Figure 9 shows the full moment tensor inversion of event 14 of Table 2. As well as event 3, it can be compared with the deviatoric inversion of Figure 6. This event, in particular, fractured more like a CLVD event having 28% of this component

and only 11% of isotropic change. Comparing the observed-synthetics fit, it can be noted that it has a variance reduction of 78%. The DC associated planes almost do not change with respect to the deviatoric inversion plotted in Figure 6.

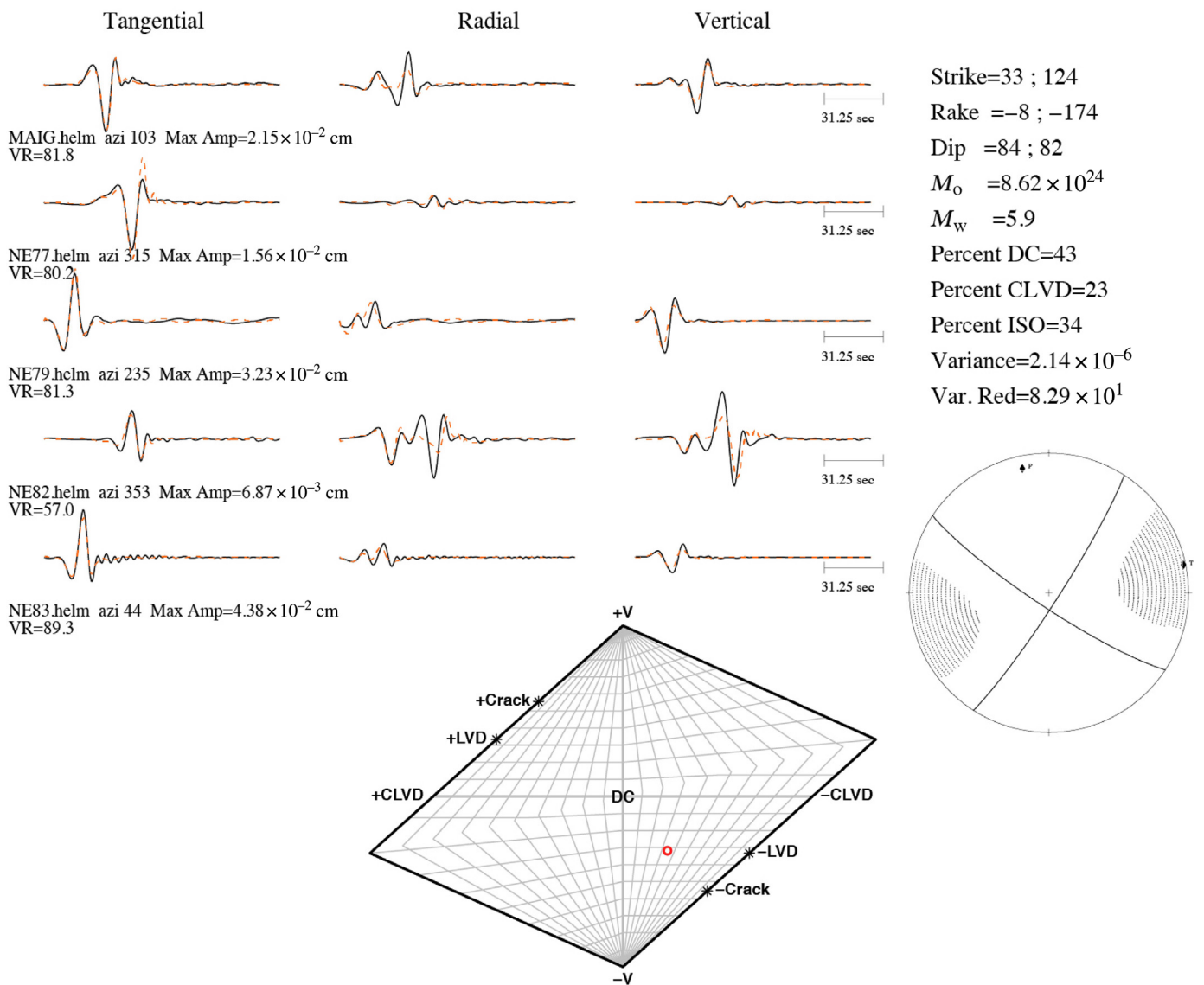
### DISCUSSION

There is enough evidence that earthquakes rupture in ways that are different than a DC. Examples of full moment tensors can be found in divergent margins, deep earthquakes, and volcanic fields. In addition, high-non-double-couple components of full moment tensors have been found in transform faults such as the GoC (Ortega *et al.*, 2013, 2016). Full moment tensors have the advantage that they may reflect the source mechanism complexity. In Figure 10, we plot the 45 full moment tensors listed in Table 4. Most of them are located within the GoC, except the one that is located in the Magdalena microplate (earthquake 5). As stated in the previous section, we present two examples of moment tensor inversions using local data. The azimuthal coverage is satisfactory having enough stations



**Figure 7.** Example of the inversion process using local and teleseismic signals for event number 14 of Table 2 located in the Gulf of California (GoC). Such as in caption of Figure 3, it is shown the focal mechanism, the moment rate function, the fault-plane solution, and the local and teleseismic signal. The black continuous lines are the observed seismograms, and the red ones are

the synthetics. The map on the upper left corner represents the location of telesismic stations used. They were chosen to homogeneously cover the epicenter. These stations are PSDB, CBN, FFC, SC15, HRV, OTAV, BBSR, TAOE, and JOHN. The color version of this figure is available only in the electronic edition.



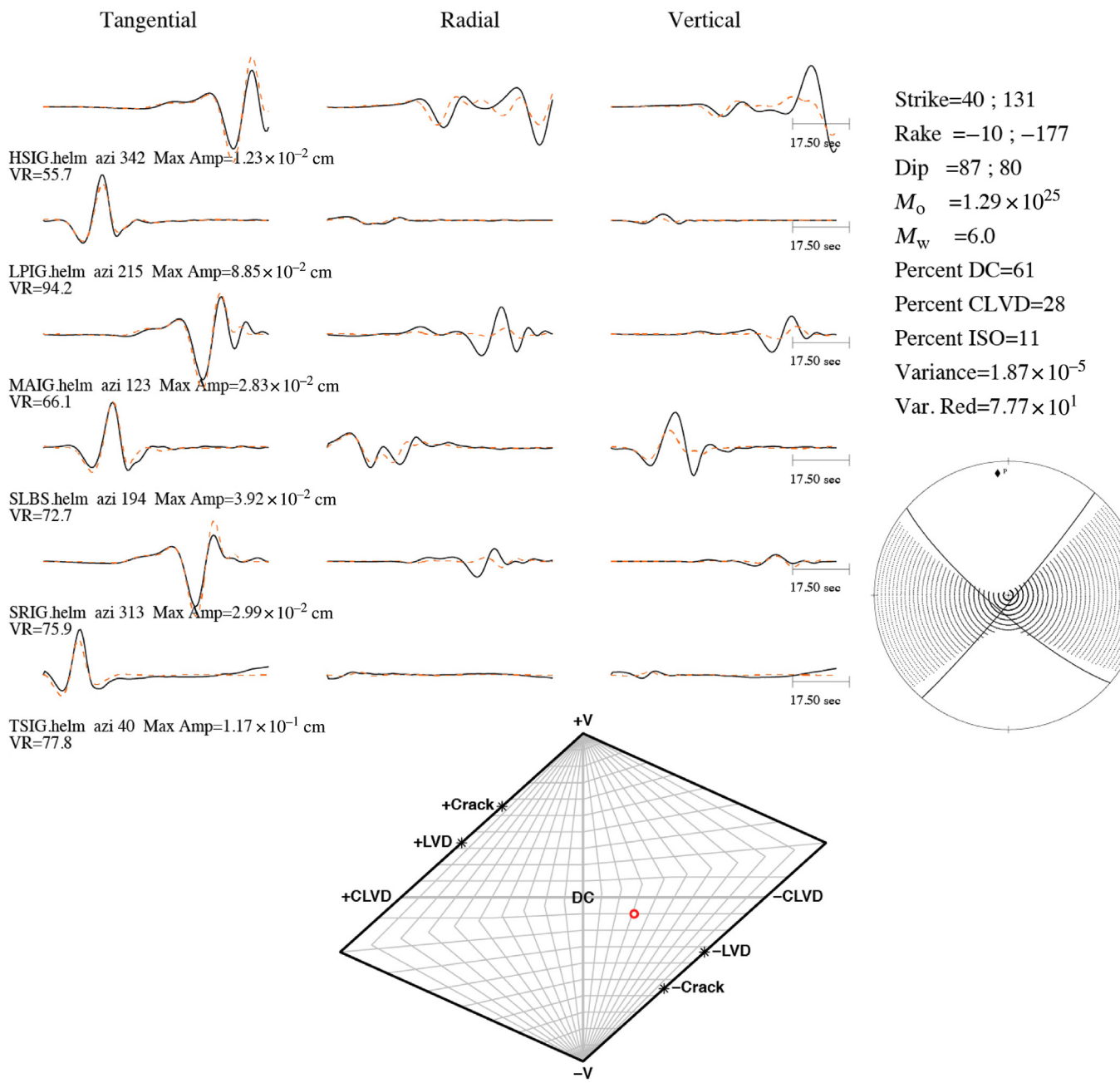
for the inversion. The good fit between the observed and synthetics seismograms gives large variance reductions, indicating that the assumed velocity model and earthquake locations are correct, and the estimated moment tensor is robust.

On the other side, a tectonic explanation for the non-double-couple components in the Gulf Extensional Province can be stated in terms of a combination of different faults interacting. For example, the 2010 Mayor–Cucapah earthquake ( $M_w$  7.2) happened in a fault that runs from California into Mexico, near Mexicali that cuts the Cucapah mountain range and ends in the Colorado delta river. This earthquake possesses a high-isotropic component that was explained as a fault made up of two different segments connected by a small extensional fault; both faults strike at the same direction but dip in opposite directions. The earthquake ruptured both segments that radiated a complex pattern of seismic waves (Wei *et al.*, 2011).

In the faults of the GoC, we observe (Fig. 10) that non-double-couple components of moment tensors are present near the corners between the transform and the extensive faults. This

**Figure 8.** Full moment tensor inversion of event 3 of the catalog of Table 2. The observed tangential, radial, and vertical waveforms are shown as solid continuous black lines, whereas the red dashed lines show the synthetic seismograms in displacement. Along with the seismograms are presented the focal mechanism and the Hudson plots. The color version of this figure is available only in the electronic edition.

observation has been explained by Ortega *et al.* (2016) in which they propose that for complex faults of two shear slip movements with different magnitudes and different directions that are interacting during the main event, the full moment tensor solution is closer to the strike and dip of the main event, and the non-double-couple part can be explained in terms of the sum of two double-couple earthquakes happening in two different faults with different directions (Fig. 11; Ortega *et al.*, 2016). However, high non-double-couple components of the moment tensor are also observed far from the corners of the extensive faults well within the transform fault. This



observation could be indicating the interaction of two or more secondary faults near the main transform fault. Sumy *et al.* (2013) show evidence of the existence of active parallel faults near the Guaymas transform fault. In the southern GoC, seismicity is registered on both the sides of the main fault. For example, Sumy *et al.* (2013) report strike-slip focal mechanisms for events located close to the Pescadero transform section. This observation suggests that parallel secondary faults may be present and active. However, they may be buried below the seafloor sediments and not mapped. More geological research could clarify the possible existence of secondary parallel faults that could be interacting in complex ways with the main fault inducing non-double-couple components in the full moment tensor of earthquakes happening in the principal

**Figure 9.** Full moment tensor inversion of event 14 of the catalog of Table 2. Such as Figure 8, the observed tangential, radial, and vertical waveforms are shown as solid continuous black lines and synthetics as the red dashed lines. Seismograms are in displacement. In addition, the focal mechanism and the Hudson plots are shown. The color version of this figure is available only in the electronic edition.

transform fault. Another explanation for non-double-couple components would involve the presence of volcanic-magma fluids. It is known that volcanoes present high isotropic components, because the magma fluids are pushing out the cone of the volcano creating an explosive radiation pattern (e.g., Miller, 1996). But unfortunately, the presence of underwater

TABLE 4  
Seismic Parameters of Full Moment Tensors Computed for the Gulf of California (GoC)

| Origin Time           |               |              |            |           |            |            |            |            |            |            |     |       |
|-----------------------|---------------|--------------|------------|-----------|------------|------------|------------|------------|------------|------------|-----|-------|
| (yyyy/mm/dd hr:mm:ss) | Longitude (°) | Latitude (°) | Depth (km) | Magnitude | Mrr        | Mtt        | Mff        | Mrt        | Mrf        | Mtf        | Exp | Event |
| 2002/10/03 16:08:29   | -108.50       | 23.30        | 15.0       | 6.3       | -136135.95 | -145329.27 | 114209.563 | -79162.195 | 46304.082  | -132854.56 | 20  | 1     |
| 2003/03/12 23:41:33   | -110.58       | 26.65        | 9.0        | 6.3       | -15105.247 | -386683.97 | 266067.344 | 48174.6641 | -50736.613 | -70374.336 | 20  | 2     |
| 2003/04/15 08:21:17   | -109.44       | 25.01        | 10.0       | 5.3       | -1767.4882 | -12170.98  | 6585.48096 | -2609.4175 | -223.98529 | -276.41873 | 20  | 3     |
| 2003/07/02 05:11:35   | -108.12       | 23.01        | 8.0        | 5.7       | -1936.9752 | -35059.012 | 7306.49561 | -2886.9561 | -6756.6118 | -12302.707 | 20  | 4     |
| 2004/02/09 09:03:46   | -112.49       | 24.93        | 8.0        | 5.5       | -9273.8662 | -10638.72  | 6258.99268 | 2342.28857 | 5903.0957  | -6611.7832 | 20  | 5     |
| 2004/02/18 10:59:18   | -108.81       | 23.72        | 9.0        | 5.9       | -18553.391 | -79308.828 | 14792.0146 | -12186.153 | -3464.3804 | -20508.66  | 20  | 6     |
| 2005/02/22 19:15:49   | -109.89       | 25.77        | 8.0        | 5.5       | -2559.7903 | -21089.375 | 13395.71   | 1237.72888 | -551.39783 | -2917.3035 | 20  | 7     |
| 2005/06/05 08:28:49   | -108.37       | 23.75        | 7.0        | 5.7       | -2955.9075 | -36438.195 | 17545.5215 | -5728.9771 | 4379.14697 | -11283.672 | 20  | 8     |
| 2006/05/28 14:02:54   | -111.00       | 26.83        | 9.0        | 5.2       | 402.289185 | -5182.5361 | 5137.85156 | 510.863708 | 274.309845 | 111.347687 | 20  | 9     |
| 2006/05/28 14:18:04   | -111.24       | 26.84        | 11.0       | 5.1       | -1311.8961 | -7840.8682 | 5746.39502 | 366.947601 | -1052.5197 | 274.37677  | 20  | 10    |
| 2006/07/30 01:20:58   | -111.25       | 26.69        | 7.0        | 5.9       | -19169.623 | -77217.672 | 49330.2891 | 7169.26807 | -18332.725 | 3344.11231 | 20  | 11    |
| 2007/02/25 15:00:42   | -110.29       | 26.21        | 7.0        | 5.8       | -12286.725 | -59568.277 | 36755.5195 | -18994.469 | -18130.93  | -4988.668  | 20  | 12    |
| 2007/03/13 02:59:01   | -110.64       | 26.14        | 9.0        | 5.9       | -22189.791 | -68058.688 | 88692.6719 | 4544.19141 | -23935.883 | 15789.8662 | 20  | 13    |
| 2007/03/28 13:21:36   | -109.69       | 25.41        | 6.0        | 5.2       | -1588.2537 | -6143.4063 | 4166.43164 | 2551.07178 | -616.71295 | -1588.15   | 20  | 14    |
| 2007/09/02 11:04:47   | -109.81       | 24.64        | 9.0        | 5.3       | -331.3949  | -8814.6084 | -118.87199 | -1053.5999 | -682.96069 | -2643.9836 | 20  | 15    |
| 2008/08/07 02:18:14   | -110.94       | 26.72        | 5.0        | 5.4       | -1945.2887 | -12741.684 | 6279.83398 | -2861.4282 | 889.660889 | -3073.0671 | 20  | 16    |
| 2009/07/03 20:30:36   | -109.73       | 25.29        | 5.0        | 5.0       | -160.63138 | -1565.1058 | 3175.72388 | -535.85284 | -710.50537 | 2120.75122 | 20  | 17    |
| 2009/07/03 09:57:01   | -109.62       | 25.37        | 7.0        | 5.3       | -554.60504 | -4044.7144 | 10834.2422 | 1373.6333  | -2738.3733 | 2156.38672 | 20  | 18    |
| 2009/07/03 11:00:16   | -109.62       | 25.22        | 5.0        | 5.8       | -600.73785 | -38550.453 | 59223.8164 | -8451.627  | -26194.938 | 9026.31934 | 20  | 19    |
| 2009/12/13 16:59:15   | -110.58       | 26.35        | 17.0       | 5.1       | -1172.5023 | -3395.9019 | 4058.58106 | 1344.44128 | 1445.61206 | -384.79742 | 20  | 20    |
| 2010/10/20 03:39:29   | -108.95       | 24.80        | 10.0       | 4.8       | 375.806854 | -2053.2537 | 1758.12744 | 546.891113 | -512.52106 | 416.923248 | 20  | 21    |
| 2010/10/20 04:15:35   | -109.19       | 24.51        | 5.0        | 5.6       | -12624.192 | -35122.148 | 13617.8623 | 5528.09717 | 3283.63403 | 34.297413  | 20  | 22    |
| 2010/10/20 06:58:14   | -109.09       | 24.52        | 8.0        | 5.8       | -9654.79   | -56992.168 | 12666.3027 | -297.77081 | -11264.066 | -2219.6633 | 20  | 23    |
| 2010/10/20 04:09:43   | -109.13       | 24.59        | 8.0        | 5.8       | -14010.163 | -66993.336 | 15963.9697 | 2740.4397  | -13492.552 | 2300.00391 | 20  | 24    |
| 2010/10/21 14:26:39   | -109.30       | 24.64        | 8.0        | 4.8       | -670.9596  | -2067.123  | 1231.05249 | -432.51059 | -294.51013 | -296.13663 | 20  | 25    |
| 2010/10/21 17:53:13   | -109.17       | 24.79        | 12.0       | 6.6       | -188561.41 | -1099153.6 | 361979.719 | 218817.953 | -315266.88 | -81540.602 | 20  | 26    |
| 2010/10/25 10:06:13   | -109.30       | 24.70        | 19.0       | 5.1       | -1589.4033 | -4253.395  | 958.824036 | -971.72998 | -191.99838 | -1100.1428 | 20  | 27    |
| 2010/10/28 02:22:25   | -108.43       | 23.18        | 8.0        | 5.6       | -5386.3062 | -24643.148 | 1552.79993 | -1443.1996 | -5016.6738 | -7855.4409 | 20  | 28    |
| 2010/12/04 23:56:22   | -109.86       | 25.42        | 7.0        | 5.0       | -802.3869  | -2199.4387 | 1150.21228 | 1103.34668 | 848.553223 | 1934.94482 | 20  | 29    |
| 2011/01/12 02:38:14   | -111.50       | 27.23        | 9.0        | 5.0       | -371.47015 | -3049.8804 | 2483.00513 | -13.93204  | 1482.04297 | -390.36716 | 20  | 30    |
| 2011/03/13 08:35:35   | -109.52       | 25.64        | 11.0       | 4.8       | -36.609283 | -1475.8827 | 1782.91614 | 628.123657 | 74.922363  | -214.95198 | 20  | 31    |
| 2011/04/26 21:10:25   | -111.40       | 27.60        | 7.0        | 5.5       | -3691.8003 | -20927.537 | 3831.46509 | 387.440002 | -1787.8727 | -5156.1001 | 20  | 32    |
| 2011/07/26 17:44:21   | -109.54       | 25.09        | 8.0        | 6.0       | -15522.828 | -119501.26 | 52251.5195 | -34316.145 | -16494.143 | -9633.8027 | 20  | 33    |
| 2012/08/02 22:13:16   | -109.62       | 25.02        | 7.0        | 5.0       | -174.35577 | -3039.3174 | 1055.30273 | 863.57959  | 843.473877 | -558.31464 | 20  | 34    |
| 2012/10/08 06:26:23   | -109.61       | 25.09        | 4.0        | 5.9       | -15429.327 | -81552.844 | 45157.5391 | -11870.923 | -13159.861 | -11155.736 | 20  | 35    |
| 2013/01/13 16:28:28   | -110.16       | 25.82        | 2.0        | 5.6       | -1760.1288 | -26102.078 | 15817.5889 | 5718.95215 | -1334.7758 | -2308.0479 | 20  | 36    |
| 2013/10/19 17:54:57   | -110.36       | 25.96        | 12.0       | 6.5       | 40737.8398 | -686103.06 | 549360.063 | 111204.883 | -28501.666 | -14357.383 | 20  | 37    |
| 2014/07/22 06:50:25   | -110.46       | 25.90        | 5.0        | 5.0       | -714.37567 | -3507.9988 | 2713.48218 | -16.225306 | 882.150696 | -1099.1439 | 20  | 38    |
| 2014/08/10 18:46:17   | -111.63       | 27.68        | 6.0        | 5.6       | -3321.3418 | -25989.988 | -331.5903  | 2196.93189 | 5171.30518 | -6817.1348 | 20  | 39    |

(continued)

TABLE 4 (Continued)

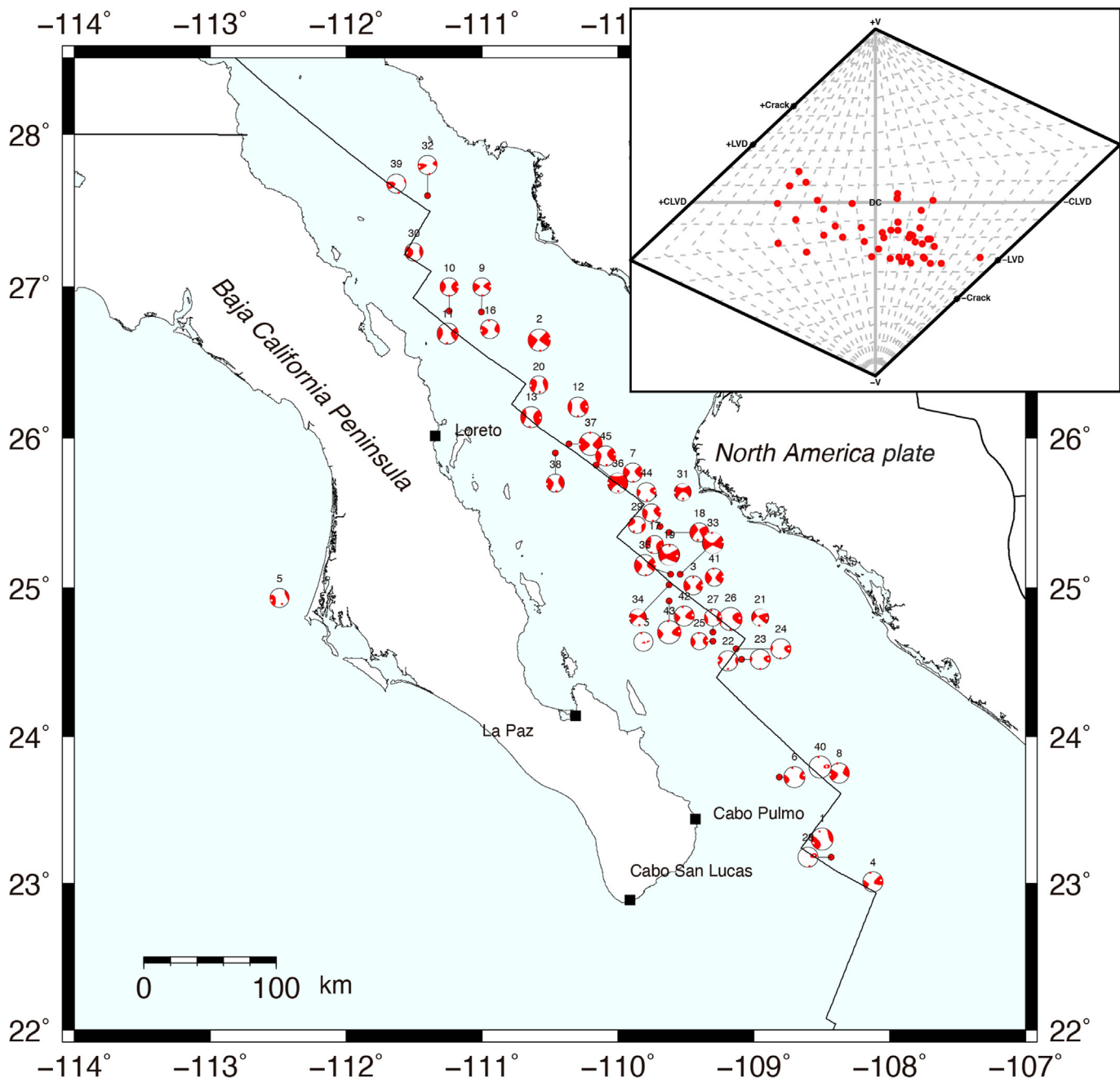
| Origin Time<br>(yyyy/mm/dd hr:mm:ss) | Longitude (°) | Latitude (°) | Depth (km) | Magnitude | Mrr        | Mtt        | Mff        | Mrf        | Mtp        | Event            |
|--------------------------------------|---------------|--------------|------------|-----------|------------|------------|------------|------------|------------|------------------|
| 2014/10/08 02:40:52                  | -108.51       | 23.79        | 5.0        | 6.2       | -21642.279 | -218494.92 | 4328.2417  | 3396.32495 | -34513.09  | 20 40            |
| 2015/09/13 07:40:39                  | -109.29       | 25.07        | 8.0        | 5.2       | -465.66399 | -6086.8374 | 6442.93164 | -719.47711 | -826.74738 | -635.82471 20 41 |
| 2015/09/13 07:57:33                  | -109.51       | 24.81        | 5.0        | 5.6       | -2599.9292 | -25495.295 | 9215.0752  | -234.71562 | -2196.2012 | -5473.7451 20 42 |
| 2015/09/13 08:14:08                  | -109.62       | 24.91        | 4.0        | 6.6       | -107858.46 | -879812.69 | 35770.375  | 124249.188 | 128451.508 | -143174.72 20 43 |
| 2016/10/13 03:55:12                  | -109.79       | 25.64        | 11.0       | 5.4       | -3543.9058 | -13286.621 | 3707.38306 | 1954.20032 | 74.829742  | -1914.6567 20 44 |
| 2017/03/29 15:15:23                  | -110.09       | 25.88        | 10.0       | 5.7       | -6618.502  | -31526.563 | 39627.9844 | 5721.80078 | -3697.2737 | -7299.6099 20 45 |

Moment-tensor elements in the standard spherical coordinate system. Moment-tensor elements are given in Newton-m. Tensor elements in cartesian components are equivalent to: Mrr = Mzz, Mtt = Mxx, Mff = Myy, Mrt = Mxz, Mrf = -Myz, and Mtp = -Mxy.

volcanoes has not been observed or reported in the literature for the Gulf of California. The existence of volcanoes has been only reported along the peninsula of Baja California, and their origin are associated to postsubduction volcanism (Di Luccio *et al.*, 2014). In Figure 10 (inset), the Hudson plot is shown for the full moment tensors of events computed for the southern GoC. It can be noted that the red dots of the  $T-k$  diagram are distributed in the negative  $k$  axis, that is, it corresponds to negative cracks (implosions). In fact, a  $k > 0$  would have more physical meaning, because it would be related with an explosive source; in this case, where we observe negative  $k$  the good fit between the observed and synthetic seismograms cannot be related with a physically real seismic source. Therefore, we interpret the Hudson plot obtained as a result of parallel (or perpendicular) geologic faults interacting.

Few earthquakes of moderate magnitude ( $M_w$  5–6) have been studied to know their rupture process. Examples of this kind of studies are the Hokubu intraplate earthquake of  $M_w$  5.2 (Kimura and Kakehi, 2005); the work of Rodríguez-Lozoza (2008) that analyzes four moderate earthquakes in the central GoC; and the San Pedro Martir earthquake of magnitude 6.5 located in the north of the Gulf Extensional Province (Quintanar *et al.*, 2019). This is the first time that more finite-source inversion has been achieved in the GoC. In this study, we used broadband stations located in the area and teleseismic data when possible. Figure 12 shows 25 source-rupture processes that are compiled together in a map of the Gulf of California for comparison. The numbers follow the list of Table 2 and are ordered chronologically as stated before. The plot presents the focal input mechanism in which the compressive quadrants are colored in red. The focal mechanism that is used as input is assumed to be a DC. The blue line indicates the position and length of the fault plane used in the inversion scaled to the map. We can appreciate that, in general, for the Gulf Extensional Province the source-rupture processes tend to be simple, with the rupture surrounding the hypocenter (e.g., earthquakes 8 and 14). In some other cases, more heterogeneities in the rupture-source process can be observed (e.g., earthquakes 3, 5, and 22).

In general, the rupture processes observed tend to be simple, with displacements concentrated mainly near the hypocenter (yellow star) not showing a clear directivity. One explanation for these observations could rely on the moderate magnitude of the earthquakes analyzed. Because they are mainly earthquakes of magnitude between 5 and 6, their ruptures do not propagate enough from the hypocenter (between 6 and 13 km, see Table 3) to define a clear direction of propagation, so displacements tend to concentrate around the hypocenter. However, bigger than magnitude 6 earthquakes tend to show more directivity (e.g., earthquake 18) and heterogeneities in the source rupture. Earthquake listed with number 15 in Table 3, which is a magnitude 7, shows a clear directivity toward the southeast. This is due to its long-rupture

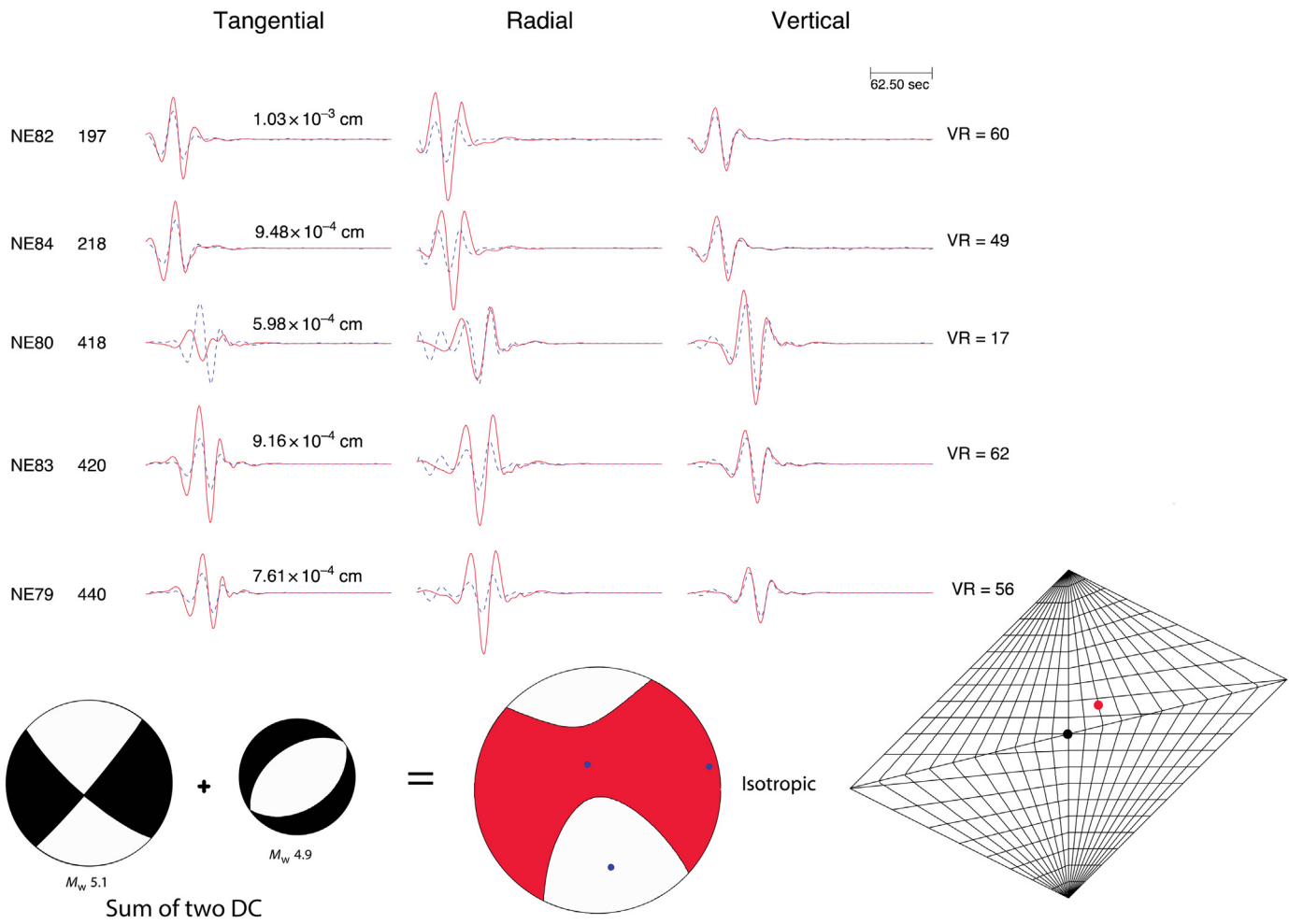


propagation of  $\sim 77$  km. Another aspect to considerate in the interpretation is that complex sources are common in the seismicity of the Gulf of California (e.g., Ortega *et al.*, 2013, 2016), and this complexity is not considered in the inversion algorithm of Yagi *et al.* (1999) that assumes a pure DC (Yagi *et al.*, 1999; Rodríguez-Lozoya *et al.*, 2008) hiding detailed information about the source. It has been shown that high non-double-couple components are present in the seismicity of the GoC (Fig. 10), implying the interaction of two or more faults during the earthquake. This complex rupture process that is accommodating deformation in multiple faults that are interacting between them is not considered in the inversion.

**Figure 10.** Full moment tensors computed for the southern Gulf of California. Numbers indicate the position of each event according to the catalog of Table 4. Inset shows Hudson plot for the events in the map. The color version of this figure is available only in the electronic edition.

## CONCLUSIONS

Rupture process is investigated systematically for earthquakes with  $M > 5.0$  in the period 2000–2020 that occurred in the GoC. We start obtaining the best DC using the Dreger and Helmberger (1993) method. Afterward, we used 25 focal mechanisms with a homogeneous azimuthal coverage and VR over 75% as input to the Yagi *et al.* (1999) inversion program to



obtain the slip distribution on the fault plane; this analysis was performed using regional and teleseismic data. The study shows that seismic sources are simple for moderate magnitudes ( $M$  5–6). The largest slips occur near the hypocenter, and they do not exhibit a preferential direction of the rupture. They are more heterogeneous for larger magnitudes. The mean stress-drop values estimated assuming a Haskell rectangular fault model are lower than 1 MPa, indicating a low seismic coupling and considerable heterogeneity in the medium. In addition, we computed full moment tensors to investigate the non-double-couple component of the faulting in the GoC; our results show a high percentage of CLVD component in the moment tensor calculated for 45 earthquakes. Several authors have shown that faulting in the GoC basin produces significant non-double-couple components. These high non-double-couple components have been interpreted as complex ruptures or faulting in the Gulf. The complexity could involve two or multiple faults interacting.

## DATA AND RESOURCES

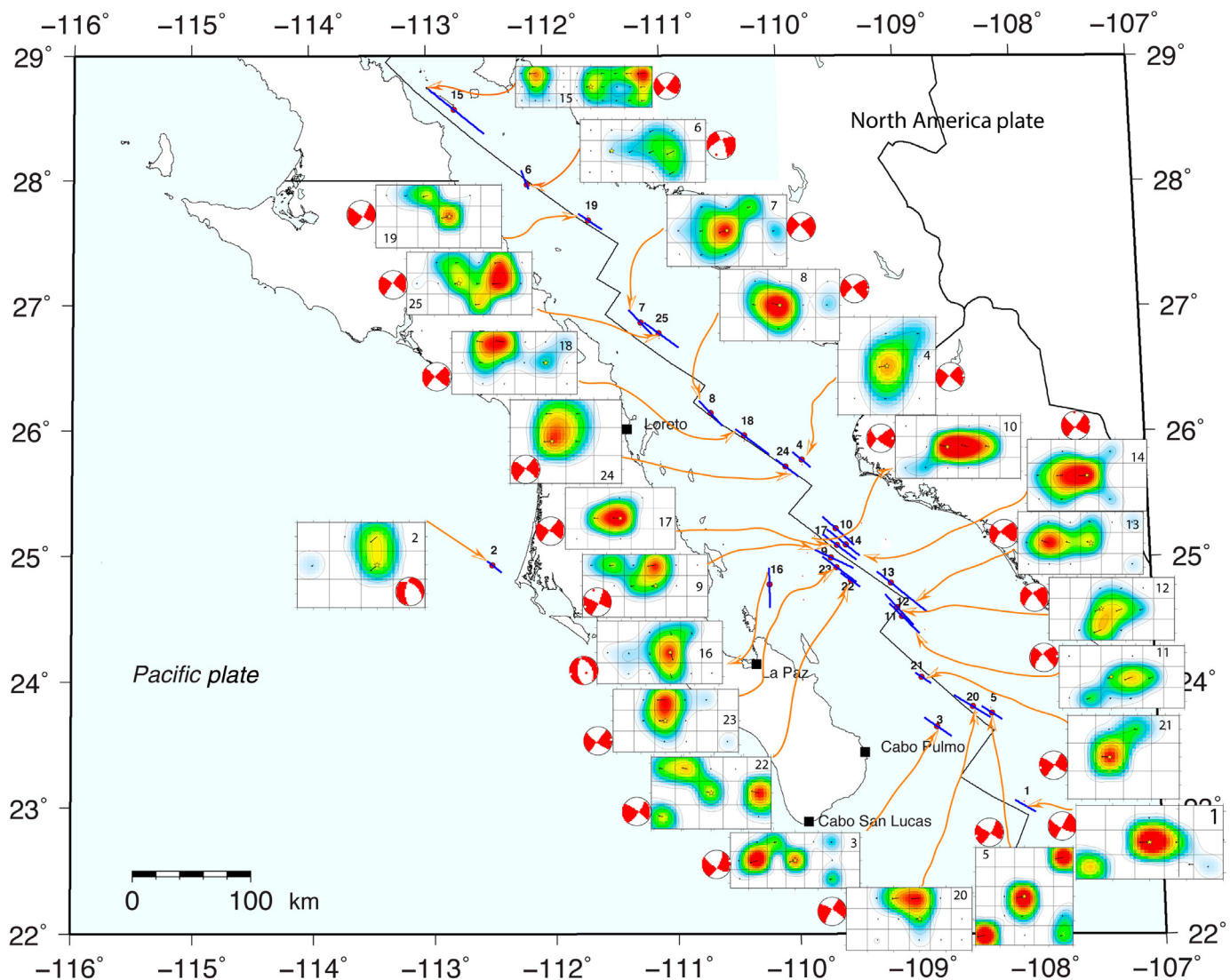
Seismograms used in this study were collected from Network of Autonomously Recording Seismograms (NARS-Baja), NR; Red Sismológica de Banda Ancha del Golfo de California (RESBAN),

**Figure 11.** Synthetic example showing how two double couples produce a moment tensor with a large non-double-couple component. In this figure, the sum of a strike slip with a normal focal mechanism with different magnitudes produces the red color focal mechanism plot. The figure is modified from Ortega *et al.* (2016). The color version of this figure is available only in the electronic edition.

RB; and Servicio Sismológico Nacional (SSN), MX networks. Data from Red Sísmica del Noroeste de México (RESNOM) were provided by Raúl Castro from Centro de Investigación Científica y de Educación Superior de Ensenada (CICESE). Data from SSN were provided by Caltech using a file transfer protocol (FTP) service. FTP access can be obtained by contacting Arturo Iglesias at Universidad Nacional Autónoma de México (UNAM). NARS data ([Utrecht University \[UU Netherlands, 1983\]](#)) were downloaded directly from Incorporated Research Institutions for Seismology Data Management Center (IRIS-DMC) at <https://www.iris.edu>. Some plots were made using the Generic Mapping Tools (GMT) version 4.2.1 (v.4.2.1) (<https://www.soest.hawaii.edu/gmt>; Wessel and Smith, 1998). All websites were last accessed in February 2021.

## DECLARATION OF COMPETING INTERESTS

The authors acknowledge that there are no conflicts of interest recorded.



## ACKNOWLEDGMENTS

The authors are thankful to everyone in the staff of Mexico's Servicio Sismológico Nacional (SSN) for the operation and data acquisition and distribution from the broadband network. The authors want to thank Centro de Investigación Científica y de Educación Superior de Ensenada (CICESE), Unidad La Paz for their financial support (Internal Project 691115) and Consejo Nacional de Ciencia y Tecnología (Conacyt; Project 97), and Raúl Castro from CICESE Ensenada for providing data from the Red Sísmica del Noroeste de México (RESNOM) array. We also want to thank two anonymous reviewers for their comments that helped to improve the manuscript. Some figures were made using the Generic Mapping Tools (GMT) package (Wessel and Smith, 1998).

## REFERENCES

- Akaike, H. (1980). Likelihood and Bayes procedure, in *Bayesian Statistics*, J. M. Bernardo, M. H. DeGroot, D. V. Lindley, and F. M. Smith, (Editors) University of Press, Valencia, Spain, 143–166.
- Atwater, T. M. (1970). Implications of plate tectonics for the Cenozoic tectonic evolution of western North America, *Geol. Soc. Am. Bull.* **81**, 3513–3536.
- Atwater, T. M. (1989). Plate tectonic history of the northeast Pacific and western North America, in *The Geology of North America: The Northeastern Pacific Ocean and Hawaii*, E. L. Winterer, D. M. Hussong, and R. W. Decker (Editors), Geological Society of America, Boulder, Colorado, 21–72.
- Atwater, T., and J. M. Stock (1998). Pacific–North America plate tectonics of the Neogene southwestern United States: An update, *Int. Geol. Rev.* **40**, 375–402.
- Castro, R. R., D. D. Carciumaru, C. Magali, V. William, G.-H. Hector, M. Antonio, and P.-V. Arturo (2021). Seismicity in the Gulf of California, Mexico, in the period 1901–2018, *J. South Am. Earth Sci.* **106**, 103087, doi: [10.1016/j.jsames.2020.103087](https://doi.org/10.1016/j.jsames.2020.103087).

**Figure 12.** Rupture-process models of 25 earthquakes in the Gulf extensional province. The inversions were obtained using the Yagi et al. (1999) algorithm. In addition, focal mechanism used is plotted next to the models. The red quadrants on focal mechanism plots represent compressions. The blue lines indicate the position of the plane used for the inversion. Numbers refer to the catalog of Table 2. The color version of this figure is available only in the electronic edition.

- Castro, R. R., J. M. Stock, E. Hauksson, and R. W. Clayton (2017). Active tectonics in the Gulf of California and seismicity ( $M > 3.0$ ) for the period 2002–2014, *Tectonophysics* **719/720**, 4–16, doi: [10.1016/j.tecto.2017.02.015](https://doi.org/10.1016/j.tecto.2017.02.015).
- Clayton, R. W., J. Trampert, C. Rebollar, J. Ritsema, P. Persaud, H. Paulssen, X. Perez-Campos, A. van Wettum, A. Perez-Vertti, and F. DiLucio (2004). *The NARS-Baja Seismic Array in the Gulf of California Rift Zone, MARGINS, Newsletter*, Vol. 13, Washington University, St. Louis, Missouri, 1–4.
- Coyán, M. M., J. R. Arrowsmith, P. Umhoefer, J. Coyan, G. Kent, N. Driscoll, and G. M. Gutiérrez (2013). Geometry and quaternary slip behavior of the San Juan de los Planes and Saltito fault zones, Baja California Sur, Mexico: Characterization of rift-margin normal faults, *Geosphere* **9**, no. 3, 426–443.
- DeMets, C., and T. H. Dixon (1999). New kinematic models for Pacific-North America motion from 3 Ma to present, I: Evidence for steady motion and biases in the NUVEL-1A model, *Geophys. Res. Lett.* **26**, 1921–1924.
- Di Luccio, F., P. Persaud, and R. W. Clayton (2014). Seismic structure beneath the Gulf of California: A contribution from group velocity measurements, *Geophys. J. Int.* **199**, no. 3, 1861–1877, doi: [10.1093/gji/ggu338](https://doi.org/10.1093/gji/ggu338).
- Dickinson, W., and W. Snyder (1979). Geometry of subducted slabs related to San Andreas transform, *J. Geol.* **87**, 609–627.
- Dixon, T., F. Farina, C. DeMets, F. Suarez-Vidal, J. Fletcher, B. AzuaMarquez-, M. Miller, O. Sanchez, and P. J. Umhoefer (2000). New kinematic models for Pacific-North America motion from 3 Ma to present, II: Evidence for a Baja California shear zone, *Geophys. Res. Lett.* **27**, 3961–3964, doi: [10.1029/2000GL008529](https://doi.org/10.1029/2000GL008529).
- Dreger, D. S., and D. V. Helmberger (1990). Broadband modeling of local earthquakes, *Bull. Seismol. Soc. Am.* **80**, 1162–1179.
- Dreger, D. S., and D. V. Helmberger (1991). Complex faulting deduced from modeling of the 28 February 1990 upland (ML 5.2), *Bull. Seismol. Soc. Am.* **89**, 1129–1144.
- Dreger, D. S., and D. V. Helmberger (1993). Determination of source parameters at regional distances with three-component sparse network data, *J. Geophys. Res.* **98**, 8107–8125.
- Dziewonski, A. M., T.-A. Chou, and J. H. Woodhouse (1981). Determination of earthquake source parameters from waveform data for studies of global and regional seismicity, *J. Geophys. Res.* **86**, 2825–2852, doi: [10.1029/JB086iB04p02825](https://doi.org/10.1029/JB086iB04p02825).
- Ekström, G., M. Nettles, and A. M. Dziewonski (2012). The global CMT project 2004–2010: Centroid-moment tensors for 13,017 earthquakes, *Phys. Earth Planet. In.* **200/201**, 1–9, doi: [10.1016/j.pepi.2012.04.002](https://doi.org/10.1016/j.pepi.2012.04.002).
- Fletcher, J. M., and L. Munguía (2000). Active continental rifting in southern Baja California, México: Implications for plate motion partitioning and transition to seafloor spreading in the Gulf of California, *Tectonics* **19**, 1107–1123.
- Ford, S. R., D. S. Dreger, and W. R. Walter (2009). Identifying non-double couple events using a regional moment tensor inversion, *J. Geophys. Res.* **114**, no. B1, doi: [10.1029/2008JB005743](https://doi.org/10.1029/2008JB005743).
- Goff, J. A., E. A. Bergman, and S. C. Solomon (1987). Earthquake source mechanism and transform fault tectonics in the Gulf of California, *J. Geophys. Res.* **92**, no. B10, 10,485–10,510.
- González, M., A. Vidal, and L. Munguía (2006). An ML Scale for the La Paz-Los Cabos region, Baja California Sur, Mexico, *Bull. Seismol. Soc. Am.* **96**, no. 4A, 1296–1304, doi: [10.1785/0120050196](https://doi.org/10.1785/0120050196).
- Hartzell, S. H., and T. H. Heaton (1983). Inversion of strong ground motion and teleseismic waveform data for the fault rupture history of the 1979 Imperial valley, California earthquake, *Bull. Seismol. Soc. Am.* **73**, 1553–1583.
- Haskell, N. A. (1964). Total energy and energy spectra density of elastic waves from propagation faults, *Bull. Seismol. Soc. Am.* **54**, 1811–1841.
- Hudson, J. A., R. G. Pearce, and R. M. Rogers (1989). Source type plot for inversion of the moment tensor, *J. Geophys. Res.* **94**, no. B1, 765–774.
- Huesca-Pérez, E., E. Gutierrez-Reyes, R. W. Valenzuela, A. Husker, and S. Mayer (2021). 3-D travel-time tomography of southernmost Baja California peninsula, *J. South Am. Earth Sci.* **105**, 102966, doi: [10.1016/j.jsames.2020.102966](https://doi.org/10.1016/j.jsames.2020.102966).
- Jost, M. L., and R. B. Herrmann (1989). A student's guide to and review of moment tensors, *Seismol. Res. Lett.* **60**, no. 2, 37–57.
- Kimura, T., and Y. Kakehi (2005). Rupture process of the 2001 Hyogo-ken Hokubu, Japan, earthquake (Mw 5.2) and comparison between the after-shock activity and the static stress changes, *Bull. Seismol. Soc. Am.* **95**, 145–158, doi: [10.1785/0120040012](https://doi.org/10.1785/0120040012).
- Kohketsu, K. (1985). The extended reflectivity method for synthetic near-field seismograms, *J. Phys. Earth* **33**, 121–131.
- López-Pineda, L., and C. J. Rebollar (2005). Source characteristics of the Mw 6.2 Loreto earthquake of 12 March 2003 that occurred in a transform fault in the middle of the Gulf of California, Mexico, *Bull. Seismol. Soc. Am.* **95**, 419–430.
- Marsaglia, K. M. (2004). Sandstone detrital modes support Magdalena Fan displacement from the mouth of the Gulf of California, *Geology* **32**, 45–48, doi: [10.1130/G20099.1](https://doi.org/10.1130/G20099.1).
- Miller, A. D. (1996). Seismic structure and earthquake focal mechanisms of the Hengill volcanic complex, SW Iceland, *Ph.D. Thesis*, University of Durham, Durham, England.
- Michaud, F., J. Y. Royer, O. Bourgois, J. Dyment, T. Calmus, B. Bandy, M. Sosson, C. Mortera-Gutierrez, B. Sichler, M. Rebolledo-Viera, et al. (2006). Oceanic-ridge subduction vs. slab break off: Plate tectonic evolution along the Baja California Sur continental margin since 15 Ma, *Geology* **34**, 13–16, doi: [10.1130/g22050.1](https://doi.org/10.1130/g22050.1).
- Minson, S., and D. Dreger (2008). Stable inversions for complete moment tensors, *Geophys. J. Int.* **174**, 585–592.
- Molnar, P. (1973). Fault plane solutions of earthquakes and direction of motion in the Gulf of California and on the Rivera fracture zone, *Geol. Soc. Am. Bull.* **84**, 1651–1658.
- Munguía, L., M. Gonzalez Escobar, S. Mayer, and A. Aguirre (2006). Seismicity and state of stress in the La Paz-Los Cabos region, Baja California Sur, Mexico, *Bull. Seismol. Soc. Am.* **96**, 624–636.
- Munguía, L., S. Mayer, A. Aguirre, I. Méndez, M. González-Escobar, and M. Luna (2016). The 2006 Bahía Asunción earthquake swarm: Seismic evidence of active deformation along the western margin of Baja California Sur, Mexico, *Pure Appl. Geophys.* **173**, 3615–3629, doi: [10.1007/s00024-015-1184-9](https://doi.org/10.1007/s00024-015-1184-9).
- Ortega, R., L. Quintanar, and E. Huesca-Pérez (2016). Geometric aspects of the full moment tensors in the Gulf of California and the Mexican east Pacific rise, *Pure Appl. Geophys.* **173**, 3595–3614.
- Ortega, R., L. Quintanar, and L. Rivera (2013). Full moment tensor variations and non-double couple characteristics of earthquakes in the Gulf of California transform fault system, *Pure Appl. Geophys.* **171**, 2805–2817, doi: [10.1007/s00024-013-0758-7](https://doi.org/10.1007/s00024-013-0758-7).

- Oskin, M., J. Stock, and A. Martín-Barajas (2001). Rapid localization of the Pacific-North America plate motion in the Gulf of California, *Geology* **29**, 459–462.
- Pacheco, J. F., and L. R. Sykes (1992). Seismic moment catalog of large shallow earthquakes, 1900 to 1989, *Bull. Seismol. Soc. Am.* **82**, 1306–1349.
- Papazachos, B., E. Scordilis, D. Panagiotopoulos, C. Papazachos, and G. Karakassis (2004). Global relations between seismic fault parameters and moment magnitude of earthquakes, *Bull. Geol. Soc. Greece* **36**, no. 3, 1482–1489, doi: [10.12681/bgsg.16538](https://doi.org/10.12681/bgsg.16538).
- Quintanar, L., R. Ortega, H. E. Rodríguez-Lozoya, and T. Domínguez-Reyes (2019). The 4 January 2006 (Mw 6.6), San Pedro Martir earthquake: Example of an earthquake for calibrating excitation and attenuation studies, *Bull. Seismol. Soc. Am.* **109**, no. 6, 2399–2414, doi: [10.1785/0120190146](https://doi.org/10.1785/0120190146).
- Rebollar, C. J., L. Quintanar, R. Castro, M. D. Steven, J. Madrid, J. N. Brune, L. Astiz, and F. Vernon (2001). Source characteristics of a 5.5 magnitude earthquake that occurred in the transform fault system of the Delfin basin in the Gulf of California, *Bull. Seismol. Soc. Am.* **91**, no. 4, 781–791.
- Rodríguez-Lozoya, H. E., L. Quintanar, R. Ortega, C. J. Rebollar, and Y. Yagi (2008). Rupture process of four medium-size earthquakes that occurred in the Gulf of California, *J. Geophys. Res.* **113**, no. B10, doi: [10.1029/2007JB005323](https://doi.org/10.1029/2007JB005323).
- Saikia, C. K. (1994). Modified frequency-wavenumber algorithm for regional seismograms using Filon's quadrature: Modelling of Lg waves in eastern North America, *Geophys. J. Int.* **118**, 142–158, doi: [10.1111/j.1365-246X.1994.tb04680.x](https://doi.org/10.1111/j.1365-246X.1994.tb04680.x).
- Severinghaus, J., and T. M. Atwater (1990). Cenozoic geometry and thermal state of the subducting slabs beneath North America, in *Basin and Range Extensional Tectonics Near the Latitude of Las Vegas, Nevada*, B. P. Wernicke (Editor), Vol. 176, Geological Society of America Memoirs, AGU, Cambridge, Massachusetts, 1–22, doi: [10.1130/MEM176-P1](https://doi.org/10.1130/MEM176-P1).
- Servicio Sismológico Nacional (SSN) (2021). *Servicio Sismológico Nacional, Instituto de Geofísica*, Universidad Nacional Autónoma de México, Mexico, doi: [10.21766/SSNMX/SN/MX](https://doi.org/10.21766/SSNMX/SN/MX) (in Spanish).
- Stock, J. M., and K. V. Hodges (1989). Pre-Pliocene extension around the Gulf of California and the transfer of Baja California to the Pacific plate, *Tectonics* **8**, 99–115.
- Sumy, D. F., J. B. Gaherty, W.-Y. Kim, T. Diehl, and J. A. Collins (2013). The mechanisms of earthquakes and faulting in the southern Gulf of California, *Bull. Seismol. Soc. Am.* **103**, 487–506, doi: [10.1785/0120120080](https://doi.org/10.1785/0120120080).
- Thorkelson, D. J. (1996). Subduction of diverging plates and the principles of slab window, *Tectonophysics* **255**, 47–63.
- Trampert, J., A. Paulseen, A. van Wettum, J. Ritsema, R. Clayton, R. Castro, C. J. Rebollar, and A. Perez-Vertti (2003). New array monitors seismic activity near Gulf of California in Mexico, *Eos Trans. AGU* **84**, 29–32.
- Utrecht University (UU Netherlands) (1983). NARS [Data set], *International Federation of Digital Seismograph Networks*, doi: [10.7914/SN/NR](https://doi.org/10.7914/SN/NR).
- Wei, S., E. Fielding, S. Leprince, A. Sladen, J. P. Avouac, D. Helmberger, E. Hauksson, R. Chu, M. Simons, K. Hudnut, et al. (2011). Superficial simplicity of the 2010 El Mayor-Cucapah earthquake of Baja California in Mexico, *Nature Geosci.* **4**, 615–618, doi: [10.1038/ngeo1213](https://doi.org/10.1038/ngeo1213).
- Wessel, P., and W. H. F. Smith (1998). New, improved version of generic mapping tools released, *Eos Trans. AGU* **79**, 579.
- Yagi, Y., M. Kikuchi, and S. Yoshida (1999). Comparison of the coseismic rupture with the aftershock distribution in the Hyuga-nada earthquake of 1996, *Geophys. Res. Lett.* **26**, 3161–3164, doi: [10.1029/1999GL005340](https://doi.org/10.1029/1999GL005340).
- Yoshida, S. (1989). Waveform inversion using ABIC for the rupture process of the 1983 Hindu Kush earthquake, *Phys. Earth Planet. In.* **56**, 389–405, doi: [10.1016/0031-9201\(89\)90172-6](https://doi.org/10.1016/0031-9201(89)90172-6).
- Yoshida, S. (1992). Waveform inversion for rupture process using a non-flat seafloor model: Application to 1986, Andreanof Islands and 1985 Chile earthquakes, *Tectonophysics* **211**, 45–59, doi: [10.1016/0040-1951\(92\)90050-G](https://doi.org/10.1016/0040-1951(92)90050-G).

---

Manuscript received 11 August 2021